SEDIMENTOLOGY the journal of the International Association of Sedimentologists

Sedimentology (2016) **63**, 586–608 doi: 10.1111/sed.12229

Preservation of meandering river channels in uniformly aggrading channel belts

WIETSE I. VAN DE LAGEWEG*†, FILIP SCHUURMAN*‡, KIM M. COHEN*§¶, WOUT M. VAN DIJK**, YASUYUKI SHIMIZU†† and MAARTEN G. KLEINHANS*

**Faculty of Geosciences, Universiteit Utrecht, PO Box 80115, 3508 TC, Utrecht, The Netherlands (E-mail: wietse.vandelageweg@gmail.com)*

†Discipline of Geography and Spatial Sciences, School of Land and Food, University of Tasmania, Private Bag 76, Hobart, Tasmania 7001, Australia

‡Department of Rivers, Deltas and Coasts, Royal HaskoningDHV, Laan 1914, Amersfoort, The Netherlands

§Department of Applied Geology and Geophysics, Deltares, Princetonlaan 6, Utrecht, The Netherlands

¶TNO Geological Survey of the Netherlands, Princetonlaan 6, Utrecht, The Netherlands

***Department of Geography, Durham University, South Road, Durham, DH1 3LE, UK*

††Division of Environmental and Resource Engineering, University of Hokkaido, Sapporo, Japan

ABSTRACT

Channel belt deposits from meandering river systems commonly display an internal architecture of stacked depositional features with scoured basal contacts due to channel and bedform migration across a range of scales. Recognition and correct interpretation of these bounding surfaces is essential to reconstruction of palaeochannel dimensions and to flow modelling for hydrocarbon exploration. It is therefore crucial to understand the suite of processes that form and transfer these surfaces into the fluvial sedimentary record. Here, the numerical model 'NAYS2D' is used to simulate a highly sinuous meandering river with synthetic stratigraphic architectures that can be compared directly to the sedimentary record. Model results highlight the importance of spatial and temporal variations in channel depth and migration rate to the generation of channel and bar deposits. Addition of net uniform bed aggradation (due to excess sediment input) allows quantification of the preservation of meander morphology for a wide range of depositional conditions. The authors find that the effect of vertical variation in scouring due to channel migration is generally orders of magnitude larger than the effect of bed aggradation, which explains the limited impact bed aggradation has on preservation of meander morphology. Moreover, lateral differences in stratigraphy within the meander belt are much larger than the stratigraphic imprint of bed aggradation. Repeatedly produced alternations of point bar growth followed by cut-off result in a vertical trend in channel and scour feature stacking. Importantly, this vertical stacking trend differs laterally within the meander belt. In the centre of the meander belt, the high reworking intensity results in many bounding surfaces and disturbed deposits. Closer to the margins, reworking is infrequent and thick deposits with a limited number of bounding surfaces are preserved. These marginal areas therefore have the highest preservation potential for complete channel deposits and are thus best suited for palaeochannel reconstruction.

Keywords Aggradation, meandering river, morphodynamic modelling, preservation, stratigraphy.

INTRODUCTION

Fluvial meander deposits form some of the largest and most architecturally complex reservoirs in the world (e.g. North, 1996; Willis & Tang, 2010; Ethridge, 2011). Palaeochannel reconstruction of the spatially complex and heterogeneous meander belt deposits on the basis of limited outcrop, core and seismic data is therefore prone to bias. The heterogeneous nature of meander deposits and resultant compartmentalization makes production of hydrocarbons from these reservoirs difficult, leaving on average more than half of the resources in place (Tyler & Finley, 1991). Much of the uncertainty in flow simulations is related to the limits in seismic resolution and the limits in borehole networks, which are the primary tools used by geologists when predicting fluvial architecture and defining a geological model. Improving the current ability to quantitatively characterize architectural elements of fluvial meander deposits for a range of sedimentary conditions will help to fill the seismic gaps and provide geologists with a new tool to construct more realistic three-dimensional (3D) geological models.

The sedimentary record of meandering rivers consists of deposits bounded by a hierarchy of erosional scour bases, depositional horizons (floodplains and palaeosols) and accretionary surfaces within bars, spanning a range of temporal and spatial scales (Miall, 1985; Holbrook, 2001). Smaller architectural elements are often nested within larger elements and bounded by contacts of different origin and magnitude (Fig. 1). Large-scale sequence stratigraphic studies use high-order valley-scale and basin-scale contacts for intra-regional correlations, while small-scale studies examining hydraulic properties and sediment movement specifically focus on first-order lamina boundaries and second-order bar surfaces. In this hierarchy of scales, third-order to sixth-order contacts correspond to bar and channel boundaries, which can often be recognized in outcrops. A large body of literature exists in which these third-order to sixth-order contacts have been linked to specific processes in order to reconstruct ancient fluvial conditions (e.g. Allen, 1983; Friend, 1983; Best & Ashworth, 1997; Ielpi & Ghinassi, 2014) and to develop facies models (e.g. Miall, 1985; Bridge, 1993).

Quantitative theoretical relations have been derived between the height of the original morphology and the formation of stratigraphic channel bounding surfaces (e.g. Allen, 1984; Paola & Borgman, 1991; Bridge & Best, 1997). These relations describe the formation of bounding surfaces as a function of: (i) the succession and magnitude of scours related to migrating channels; and (ii) the rate of net bed aggradation. In the absence of aggradation, van de Lageweg *et al.* (2013a) used a flume experiment to empirically quantify the relation between the dimensions of a meandering channel and the resultant stratigraphic architecture. The condition of zero-net aggradation that was used in this experiment is an important limit because it provides a lower bound on the fraction of the channel deposit thickness that is preserved (Paola & Borgman, 1991).

That said, the rate of aggradation of preserved sediments is usually not known. Sedimentary

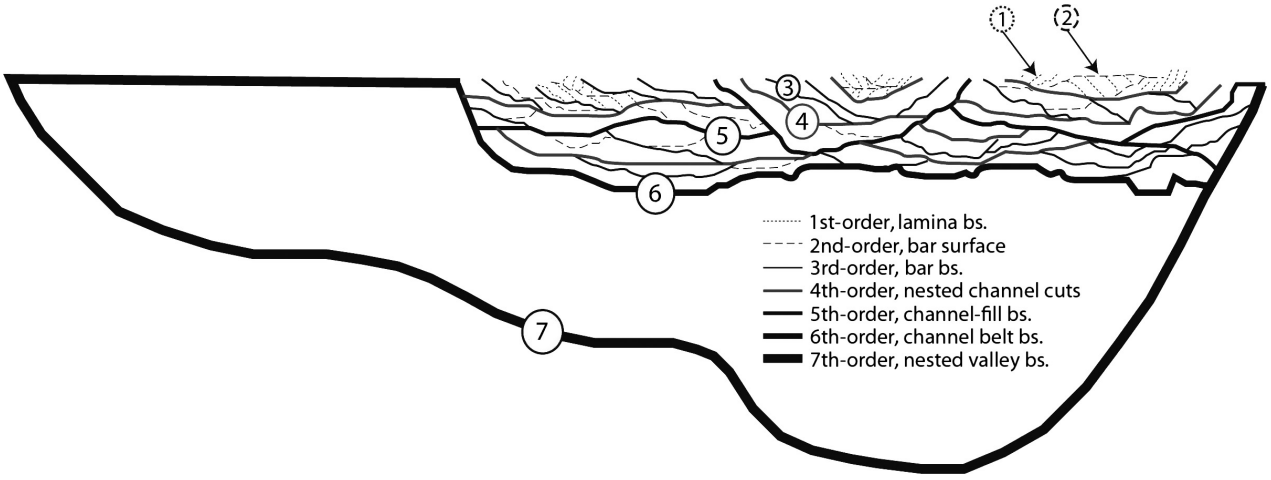

Fig. 1. The hierarchy of architectural elements. Modified from Miall (1985) and Holbrook (2001); bs, bounding surface.

records demonstrate the wide range of deposition rates in the apparent record of Earth's geological history (Sadler, 1981). Similarly, studies of short-term (single flood) to medium-term (decadal to centennial scale) meander floodplain aggradation rates highlight the large spatial and temporal fluctuations in deposition within a single environment of deposition (e.g. Walling & He, 1997; Middelkoop & Asselman, 1998; Terry *et al.*, 2002). These studies report local floodplain aggradation rates ranging anywhere from millimetres per year up to centimetres per year, and even decimetres per year in extreme cases (for example, tropical cyclone-induced floods combined with high suspended sediment concentrations). Accurate measurements of regional (entire meander belts) bed aggradation rates are also scarce. Field studies on the alluvial architecture of the Lower Rhine Valley (e.g. Erkens *et al.*, 2011) and Rhine–Meuse delta (Stouthamer *et al.*, 2011) indicate aggradation rates from 0·3 mm yr^{-1} for distal floodplain areas up to 4·2 mm yr^{-1} for local overbank aggradation rates when averaged over 10^2 to 10^3 years. In summary, net aggradation rates of a few millimetres per year are to be expected for regional systems (meander belt) while local aggradation rates at the scale of channel belts may be higher, up to centimetres per year. Therefore, temporal and spatial scale are vitally important in representing any sedimentary environment.

The process–product relationship between morphodynamics, bed aggradation and resultant stratigraphy has been explored for a range of sedimentary environments. Experimental studies comparing preservation of sedimentary structures over aggrading and non-aggrading sand beds have been conducted for subaqueous dunes (Leclair *et al.*, 1997; Leclair & Bridge, 2001; Leclair, 2002), ripples (Storms *et al.*, 1999), antidunes (Alexander *et al.*, 2001) and upper stage plane bed conditions (Bridge & Best, 1997). All of these studies found that the resultant stratigraphy did not vary systematically with aggradation rate and the authors generally could not distinguish between the sedimentary structures in the deposits formed under non-aggradational and aggradational conditions, although in certain cases the excess upstream sediment feed led to the development of a bar front with down-climbing bedforms. These experimental results have been confirmed by model results replicating migrating subaqueous bedforms for a range of aggradational conditions (Jerolmack & Mohrig, 2005), although these authors found an increased preservation for extremely high-aggradation rates. At much larger spatial and temporal scales, flume experiments have been used to study the relationship between avulsion dynamics, bed aggradation and the resultant alluvial architecture for braided river systems (e.g. Allen, 1978; Leeder, 1978; Bridge & Leeder, 1979; Bridge & Mackey, 1993; Bryant *et al.*, 1995; Mackey & Bridge, 1995; Heller & Paola, 1996; Ashworth *et al.*, 1999, 2004, 2007).

The effect of bed aggradation on meandering river systems, however, has remained largely unexplored. The relative ease of reproducing braided rivers in the laboratory (e.g. Paola *et al.*, 2001) and in numerical models (Murray & Paola, 1994; Clevis *et al.*, 2003) explains the vast amount of work done on process–product relations for braided rivers. In contrast, adequate reproduction of dynamic meandering rivers over centennial to millennial time scales has long proven challenging (Paola *et al.*, 2009; Kleinhans, 2010; Kleinhans *et al.*, 2014). Recently, significant progress in simulating this river pattern has been made both in the laboratory (e.g. Braudrick *et al.*, 2009; van Dijk *et al.*, 2012) and in numerical models (e.g. Asahi *et al.*, 2013; Schuurman *et al.*, 2015). This ability now allows examination of process–product relations for meandering rivers in much more detail for a range of known depositional conditions, in contrast to field observations where the precise depositional conditions are generally unknown. Examples of studies explicitly exploring process–product relations for meandering rivers include the role of floods (Asahi *et al.*, 2013; van de Lageweg *et al.*, 2013b) and the formation of floodplains (van Dijk *et al.*, 2013; Schuurman *et al.*, 2015). While laboratory experiments have the advantage of materiality over numerical models (Kleinhans *et al.*, 2014), laboratory replication of meandering rivers in aggradational settings across centennial to millennial time scales has proven unsuccessful so far.

The present study therefore uses the process-based numerical model 'NAYS2D' (Asahi *et al.*, 2013; Schuurman *et al.*, 2015) to simulate the evolution of a meandering channel across centennial to millennial times cales in order to systematically examine and quantify how fluctuating meander morphologies are recorded in the subsurface in response to a range of aggradational conditions: NAYS2D is the first morphodynamic model to produce river meandering without presuming a fixed relation between bank erosion and bank accretion (e.g. Willis &

Tang, 2010), allowing for a more realistic replication of meandering rivers. Specifically, the present study aims to:

1 Simulate the morphological evolution for a meandering river across centennial to millenial time scales and to examine the spatial patterns in bar erosion and deposition from a series of high-resolution digital elevation models (DEMs).
2 Quantify the 3D meander belt architecture using third-order to sixth-order bounding surfaces (Fig. 1) that were formed due to channel scouring, bar scouring and neck cut-offs.
3 Examine the relationship between bar and channel morphodynamics and the resultant meander belt architecture by comparison of sequential DEMs and the formation of bounding surfaces.
4 Quantify the effect of bed aggradation on meander belt architecture by assessing its effect on river channel deposit thickness and on the fraction of the original morphology that is preserved.

MORPHODYNAMIC MODEL SETUP

A highly sinuous meandering river and resultant alluvial architecture is simulated by the 2D fluid dynamics and morphodynamics code NAYS2D (Jang & Shimizu, 2005; Dulal *et al.*, 2010; Asahi *et al.*, 2013) to systematically test the effect of bed aggradation on meander belt stratigraphy: NAYS2D is a physics-based numerical model and simulates hydrodynamics, sediment transport and morphodynamics. The model setup was inspired by the meandering river Rhine (e.g. Stouthamer & Berendsen, 2000) and the lower Mississippi River (e.g. Fisk, 1944) because relevant parameters for designing the model such as discharge, grain size and valley gradient have been well-documented for these rivers. In addition, information about morphological behaviour (Hudson & Kesel, 2000; Kleinhans & van den Berg, 2011) and response to bed aggradation across the intended centennial to millennial time scales (Aslan & Autin, 1999; Gouw & Berendsen, 2007; Gouw, 2008) is also available for both of these river systems.

Model description

A 2D depth-averaged version of the NAYS model was used. The hydrodynamics were modelled using depth-averaged momentum and continuity equations (Asahi *et al.*, 2013). The effect of curvature-induced helical flow on the bed shear stress direction was parameterized (Engelund, 1974). Computation of the morphodynamics included sediment transport induced by the flow and bed slope, bank erosion, bar accretion and an update of the bed level. Sediment transport rate was computed by the Engelund & Hansen (1967) formulation. After each time step, the bed level was updated using the Exner equation for mass conservation of sediment (Exner, 1920, 1925; Paola & Voller, 2005).

A key feature of NAYS2D is the ability to model bank accretion and bank erosion processes explicitly. To predict bank erosion, a submodel is included in the model routine to describe the formation and removal of slump blocks that protect the bank toe against immediate slope-driven erosion (Parker *et al.*, 2011). The process of bar accretion is simplified by an effective time scale for bare sediment to become vegetated (Asahi *et al.*, 2013). In essence, the inner bank of the meandering channel is defined by the line along which the elevation of the point bar becomes identical to that of the adjacent floodplain, which is considered dry land and is excluded from the morphodynamic model domain after re-gridding. The independence of bank accretion and bank erosion allows for channel width variations, which are known to affect hydrodynamics (Zolezzi *et al.*, 2012; Frascati & Lanzoni, 2013) and sediment deposition (Eke *et al.*, 2014; van de Lageweg *et al.*, 2014) along meander bends.

Model settings and boundary conditions

In the main run, the NAYS2D model was used to simulate the alluvial channel belt architecture formed by meandering river processes without aggradation. The full model domain was 3 km wide and 10 km long. Runs started from a straight 200 m wide channel set at a gradient of 2×10^{-4} m m^{-1}. Discharge was maintained constant at 2500 m^3 sec^{-1} and a uniform grain size of 2 mm was applied, following similar simplified approaches in Schuurman *et al.* (2013) and Schuurman & Kleinhans (2015). In this approach, the constant discharge was assumed to be the dominant or effective discharge integrating all of the morphodynamic work done over a yearly hydrograph. A constant uniform bed roughness (Nikuradse k_s = 0·15 m) was used to parameterize bedform roughness.

The computational grid was initially rectangular and consisted of grid cells with a width and length of 20 m. During the run, bank erosion and bank accretion adjusted the bank lines. Regridding was performed to keep the grid boundary fitted and to maintain the transverse grid lines perpendicular to the channel centre line. The dynamic coordinate system enabled channel migration and neck cut-offs but introduced some instability over the course of the run, which limited planform development to a maximum of 668 modelled time steps. Channel neck cut-offs were modelled as an instantaneous change in planform, which could occur at any time step at which two migrating banks met. A step by step explanation of the neck-cut-off process is provided in Asahi *et al.* (2013). At the end of the model run, the dynamic coordinates of all recorded time steps were resampled to fixed Cartesian ones to generate the DEM surfaces and synthetic stratigraphy.

The influence of bed aggradation on the meander belt stratigraphic architecture was quantified by comparing the statistics extracted from the main model run (simulating zero-aggradation), to such results from the data with *post-added* excess sedimentation (simulating bed aggradation). Following Jerolmack & Mohrig (2005), simple linear bed aggradation rates were applied uniformly across the entire active domain, thus including both the channel and the floodplain. Bed aggradation rates of 1 mm yr^{-1}, 2 mm yr^{-1}, 5 mm yr^{-1} (10^3 years averaged rates also seen in natural meandering systems) and 10 mm yr^{-1}, 15 mm yr^{-1} and 20 mm yr^{-1} (very high rates, seldom sustained over 10^3 years) were post-added. While it is unlikely that the very high net aggradation rates can be sustained at a regional scale over 10^3 years, those extreme rates were explicitly included to comprehensively explore and quantify the relation between channel migration and net aggradation.

The simplified setup allows the present authors to explore and provide much-needed quantification on the effect of net aggradation on the architecture of meander belts while awaiting a better understanding and formulation of the interaction between morphodynamics and net aggradation. This numerical experiment setup neglects any altering influence that adding net aggradation could have on meander morphology, because it may potentially affect channel-bank morphodynamic interactions. This was done for a number of reasons. First, the applied net aggradation rates (approximately millimetres to centimetres of vertical thickness per year) are much smaller than the thickness that is reworked by a typical meandering channel in the model and in nature (approximately metres per major flow event). Second, in nature the interaction between meander morphodynamics and external forcings such as net aggradation (Constantine *et al.*, 2014) and subsidence (van Asselen *et al.*, 2010; Stouthamer *et al.*, 2011) is still poorly understood. Third, the present numerical model considers the floodplain next to the channel as spatially uniform anyway.

An estimate of the simulated time was required to convert bed aggradation rate to post-added bed thickness. An approximate time scale of the current simulation was based on a morphological comparison with natural meandering rivers with cohesive floodplains such as the river Rhine (e.g. Stouthamer & Berendsen, 2000; Gouw, 2008; Erkens *et al.*, 2009; Kleinhans *et al.*, 2011) and the lower Mississippi River (e.g. Fisk, 1944; Aslan & Autin, 1999; Hudson & Kesel, 2000; Gouw & Berendsen, 2007). Individual bends typically form in *ca* 250 years for the river Rhine and *ca* 500 years for the lower Mississippi River although the time scale for bend formation shows much variation for both rivers. Meanders in homolithic, cohesionless alluvium tend to evolve much faster (Bluck, 1971; Smith, 1971). This indicates that the four meander bends in the simulation herein representing sand-bed rivers encased in cohesive alluvium roughly corresponded to a millennial (*ca* 1 to 2 kyr) time scale. Therefore, it is assumed that a single model time step simulated two years of natural meander migration, which resulted in a total simulated time (668 time steps) of *ca* 1340 years. Consequently, between 1·3 m for the lowest aggradation rate of 1 mm yr^{-1} and 26·8 m for the highest aggradation rate of 20 mm yr^{-1} of bed thickness was post-added.

Characterization of stratigraphic architecture

The 668 DEMS were used to create a 3D meander belt stratigraphy. From this 3D model output, virtual cores and transects were visualized and analysed. These virtual cores corresponded to grid points within the synthetic stratigraphy and consisted of *ca* 3×10^4 individual corings at the end of the run. The analysis of the virtual cores included extraction of descriptive statistics on typical thicknesses between channel-scour and bar-scour bounding surfaces. Stratigraphic

sets are defined as depositional bodies enclosed by two successive bounding surfaces (van de Lageweg *et al.*, 2013a,b). Bounding surfaces formed by smaller scale features such as dunes and ripples were not explicitly modelled but their height can be estimated from the prescribed bed roughness as $h_{dune} = 2{\cdot}k_s$ (van Rijn, 1984). This resulted in a typical h_{dune} of 0·3 m. The present study focuses on bounding surfaces formed by bars, channels and channel cut-offs and, therefore, surfaces that were formed by an erosion event with a magnitude of 0·3 m or less were removed. In other words, the present authors ensured that the channel and bar scouring and channel cut-offs are the only formative processes feeding into the synthetic stratigraphy.

To further quantify the synthetic stratigraphic architecture, a Vertical Set Preservation Ratio (*VSPR*) was calculated. The *VSPR* quantified the average fraction of the channel deposit that was preserved. For example, if the meandering river channel deposit was on average 10 m thick and a mean set thickness of 5 m was found, the *VSPR* was 0·5.

Sensitivity analyses

Several initial and boundary conditions were varied to quantify their effect on the meander morphodynamics. A detailed description of each scenario included in the sensitivity analyses is provided in Schuurman *et al.* (2015), which specifically addresses the morphodynamic evolution of dynamic meanders in response to upstream perturbations and floodplain formation using a range of numerical models, including NAYS2D. A high-level description of the sensitivity analyses which are relevant for the current manuscript is provided below. In addition, descriptions of the sensitivity analyses in generating 3D stratigraphic architectures from composite 2D topographic surfaces and how these architectures may be affected by the methodology to post-add bed aggradation are provided.

Firstly, the effect of the upstream inflow point on meander morphodynamics was evaluated. The upstream inflow point has been identified to affect downstream meander dynamics in a range of studies (Lanzoni & Seminara, 2006; van Dijk *et al.*, 2012; van de Lageweg *et al.*, 2013a,b). Scenarios in the sensitivity analysis included: (i) no perturbation; (ii) static inflow, but offset to main channel; and (iii) lateral migration inflow. Although it is likely that the amplitude of the upstream perturbation affects downstream meander dynamics, this was not investigated here.

Secondly, the effect of the secondary spiral flow on meander morphodynamics was tested. The strength of the spiral flow is described by parameter *N*, for which values between 7 and 13 were tested; $N = 7$ is proposed in Engelund & Hansen (1967). In the morphodynamic model 'Delft3D' parameter *N* depends on Chezy roughness *C* (e.g. Lesser *et al.*, 2004; Kleinhans *et al.*, 2008) and is around $N = 10$ for a *C* between 25 $m^{1/2}$ sec^{-1} and 50 $m^{1/2}$ sec^{-1}.

Thirdly, the methodology to post-add the bed aggradation to the reworked meander belt area only introduced a systematic lateral difference in the onset of the bed aggradation signal, with the earliest onset at the axis of the meander belt and the latest onset at the margins of the meander belt. This phenomenon may have resulted in a large bed aggradation overprint in the central zone relative to the margins of the meander belt. To quantify the sensitivity of the meander belt statistics to the lateral difference in onset of the bed aggradation signal, the time series were extended artificially by mirroring the channel time series of the existing main run with respect to the meander belt axis. During this exercise, all 668 time steps of the original run were mirrored with respect to the meander belt axis, which meant that all bars and meander bends located on the right-hand side of the meander belt axis in the original run were re-located to the same position on the left-hand side of the meander belt axis and vice versa in the mirrored time series. In essence, by adding the mirrored time series to the original time series, the expansion of the meander belt and thus the systematic lateral difference in onset of the bed aggradation signal were removed. This effectively resulted in addition of the meander belt area and in replacement of synthetic stratigraphy mainly in the meander belt axis zone, and also simulated a more mature (i.e. longer activity) meander belt than the original run. Total meander belt set statistics calculated for this run thus weighed the marginal set distributions heavier than the original run.

Fourthly, the effect of the survey frequency relative to the rate of process change was tested (Lane *et al.*, 1994; Lane, 1997). The number of included composite DEMs needed to create a synthetic stratigraphy and the rate of channel migration define the resultant alluvial architecture. Therefore, the sensitivity of the presented

statistics to the number of topographic scans that were included to generate the stratigraphic architecture from composite topography was tested.

MODELLED MEANDER MORPHODYNAMICS

Effect of upstream inflow point on meander formation

The upstream inflow point had a large impact on the downstream meander dynamics. Firstly, without any upstream perturbation the initial channel remained straight. In the downstream section alternate bars were formed but these did not evolve into meander bends. Secondly, a static upstream perturbation resulted in a highly sinuous ($S \approx 1{\cdot}5$ to $2{\cdot}0$) meandering pattern. The upstream bend resulted in the formation of consecutive downstream meanders. However, sinuosity and bend amplitude decreased over time with a static upstream perturbation. Thirdly, a laterally migrating upstream inflow point resulted in an ongoing dynamic and highly sinuous ($S \approx 1{\cdot}5$ to $2{\cdot}0$) meandering pattern. It was noted that the rate of migration of the upstream inflow point had a large effect on the downstream meander dynamics, with higher meander migration and expansion rates for higher migration rates of the inflow point. Although the overall meandering pattern was very similar for all migration rates of the inflow point, meander evolution was simply faster for higher migration rates of the inflow. In the main model run, a constant migration rate of $0{\cdot}65$ m yr^{-1} with a maximum amplitude of 300 m was sufficient to maintain a dynamic meandering river pattern, while not dictating the meander dimension or geometry.

Effect of spiral flow on meander formation

The strength of the spiral flow had a large impact on the meander morphodynamics (Fig. 2). Most notably, neck cut-offs took place for the runs with a high spiral flow intensity (Fig. 2A: parameter N of 13 and Fig. 2B: parameter N of 11) but not for the run with a lower spiral flow intensity (Fig. 2C: parameter N of 7).

The descriptive parameters of the meandering planform also reflected the effects of the strength of the spiral flow (Fig. 3). Sinuosity increased to a maximum of *ca* 2 for the runs with a parameter N of 13 and 11 (Fig. 3A). The increase in sinuosity for the run with a parameter N of 7 was more gradual and reached a lower maximum sinuosity of $1{\cdot}7$. In contrast, the average length of a meander was highest for the run with a parameter N of 7 reaching an average length of *ca* 2000 m (Fig. 3B). The runs with a parameter

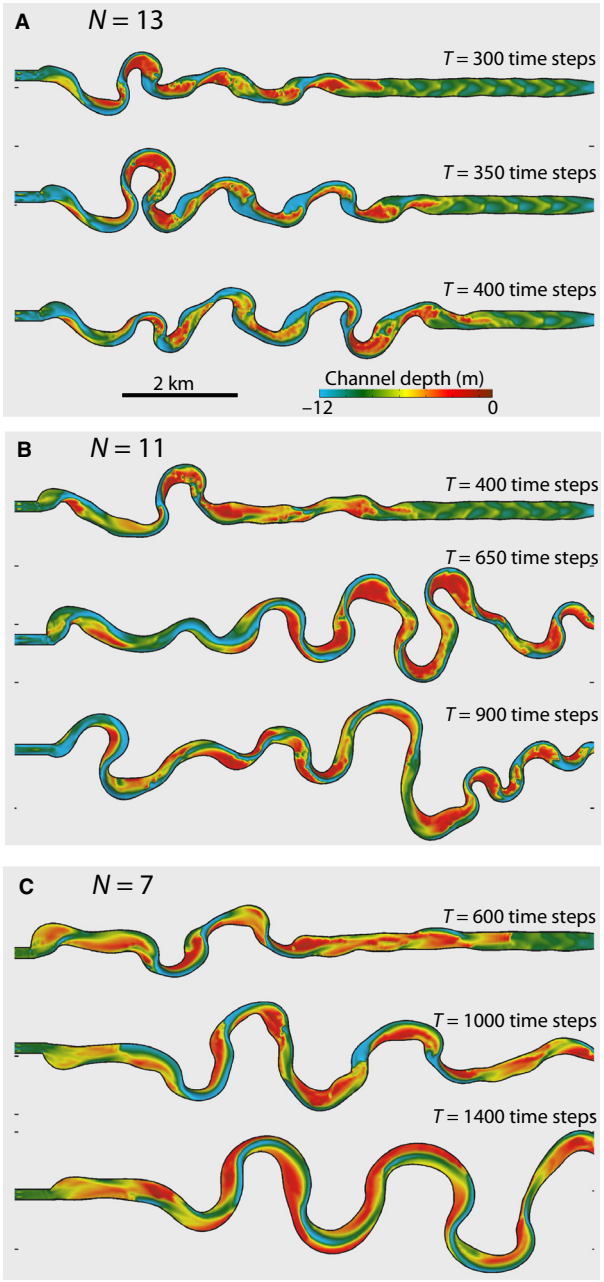

Fig. 2. Sensitivity of meandering river pattern to model parameter N (Eq. 1). This parameter quantifies the strength of the spiral flow, with a stronger spiral flow for a higher N. (A) Channel evolution for $N = 13$. (B) Channel evolution for $N = 11$. (C) Channel evolution for $N = 7$.

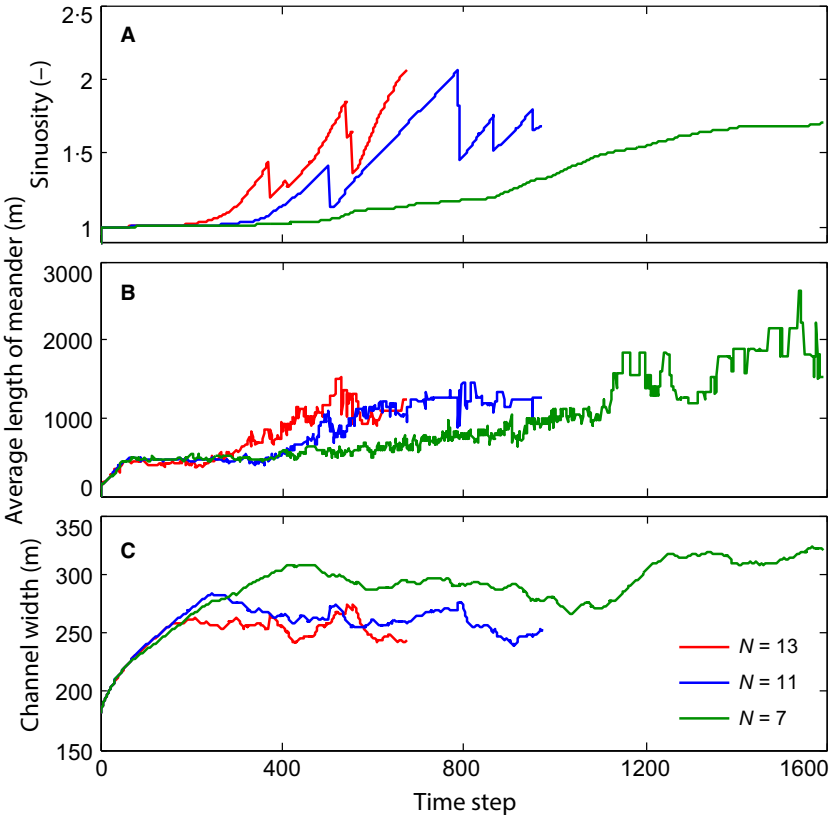

Fig. 3. Descriptive statistics of the meander pattern presented in Fig. 2 for three model runs with a varying strength of the spiral flow (parameter N, Eq. 1). (A) Time series of sinuosity S. (B) Time series of the average length of a meander. (C) Time series of the average channel width. Note that cut-offs occur for $N = 11$ and $N = 13$, as indicated by the sudden jumps in sinuosity in (A), but not for the run with $N = 7$. Note that discharge, grain size and bed roughness are constant.

N of 13 and 11 reached an average meander length of *ca* 1200 m. Similarly, the meandering channel was widest for the run with the weakest spiral flow ($N = 7$) reaching a width of *ca* 325 m and remained narrower for the runs with a stronger spiral flow ($N = 11$ and 13) with an average width of *ca* 250 m (Fig. 3C).

In summary, a stronger spiral flow resulted in the occurrence of neck cut-offs and a faster evolution of the meandering river (Fig. 2). At the same time, the overall meandering planform remained very similar for the three runs as indicated by the descriptive parameters (Fig. 3). To minimize run time and to maximize the dynamics of the meandering river, the present authors continued to use $N = 13$ to quantify the effect of bed aggradation on the preservation of meander morphology.

Main model run

Figure 4 shows the modelled meander belt evolution. The initial straight channel developed into a highly sinuous ($S \approx 1{\cdot}5$ to $2{\cdot}0$) meandering river. The meander bends were free to expand laterally and meander bend expansion was the most common meander planform evolution. The sinuous single-thread channel was on average 8 m deep but locally reached depths up to *ca* 20 m. The deepest parts corresponded to outer bends, whereas inner bends were notably shallower. Channel width also varied greatly with an average of 250 m (Fig. 3C) but locally the channel was only 180 m wide. These channel dimensions resulted in a typical channel width to depth ratio between 20 and 30, which is representative for mixed-load single-thread sinuous channels; for example, in commonly applied classification schemes (Schumm, 1985; Kleinhans & van den Berg, 2011) and in real-world alluvial river settings such as the Mississippi River (Hudson & Kesel, 2000) and the river Rhine (Erkens *et al.*, 2009, 2011). In addition, width to depth ratios between 20 and 30 also overlap significantly with the initial aspect ratio of channels cut into alluvium without further change (Gibling, 2006). Individual meanders had a typical length of 1000 to 1200 m (Fig. 3B) with a maximum meander length of *ca* 1500 m. The meander belt width was generally between 1000 m and 1500 m.

The simulation showed initially high-mode bars (Crosato & Mosselman, 2009) typically with three bars migrating in parallel, which

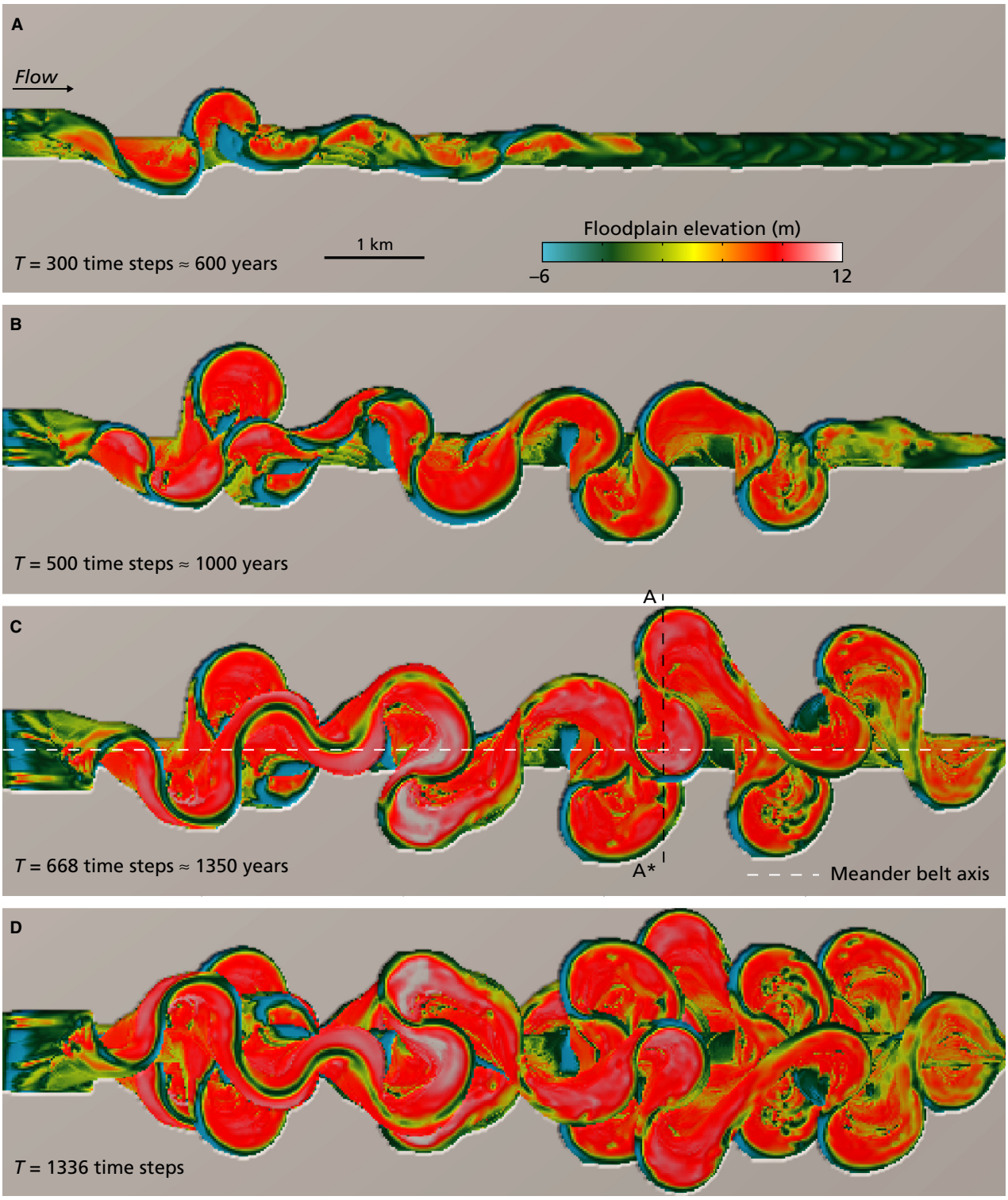

Fig. 4. Meander belt formation in the main model run. Simulation for this main run starts from an initial straight channel and resulted in a highly sinuous ($S \approx 1{\cdot}5$ to $2{\cdot}0$) meandering channel after 668 time steps (A, B and C). In an auxiliary run (D), the channel time series of this main model run was mirrored with respect to the meander belt axis, indicated in (C). This resulted in addition of the meander belt area and in replacement of synthetic stratigraphy mainly in the meander belt axis zone. Total meander belt set statistics calculated for this run thus weigh the marginal set distributions heavier than the main run. Note that the amplitude and rate of the upstream perturbation are constant.

were succeeded by more steady alternate bars that ultimately evolved into point bars (Fig. 4). The high-mode bars were formed in the initial straight channel and were typically *ca* 100 m long and wide with a height of a few metres (Fig. 4A, downstream section). Alternate bar formation was triggered by a static upstream bar and was unrelated to the high-mode bars (Fig. 4A, upstream section). Alternate bars were much larger than the high-mode bars with a typical length between 500 m and 1000 m, a width of *ca* 100 m and a height typically between 5 m and 10 m. The alternate bars then gradually graded into larger scale point bars with a typical length and width between 1000 m and 1200 m and a typical height of *ca* 10 m (Fig. 4B and C). Point bars sometimes showed undulating surfaces, also known as 'ridge and scroll' topography. When present, point bar ridges and scrolls were generally better developed towards the margins of the point bar with a typical spacing between consecutive ridges of *ca* 100 m and 200 m and subtle elevation differences between ridges and scrolls of sub-metre scale.

Dominant morphological processes were lateral channel migration and neck cut-off (Fig. 4). The average lateral channel migration rate was 2·5 to 5·0 m yr^{-1}. Differences in channel curvature resulted in highly variable migration rates with maximum rates up to 20 m yr^{-1}. The channel was locally straightened due to neck cut-off from *ca* 350 time steps (≈ 700 years) onwards. Four such neck cut-offs occurred and their temporally straightened sections re-evolved into new meander bends.

A key result is that most of the morphological activity for the simulated meandering river took place in the centre of the meander belt. In this zone, point bar deposits that developed earlier in the run were reworked multiple times by cut-offs that occurred later in the run. Closer to the margins of the meander belt, reworking occurred less frequently.

MEANDER BELT STRATIGRAPHIC ARCHITECTURE

In the main model run herein, the varying depths as well as the succession of incising and migrating channels within the meander belt determined the formation of bounding surfaces and stratigraphic architecture (Fig. 5). The

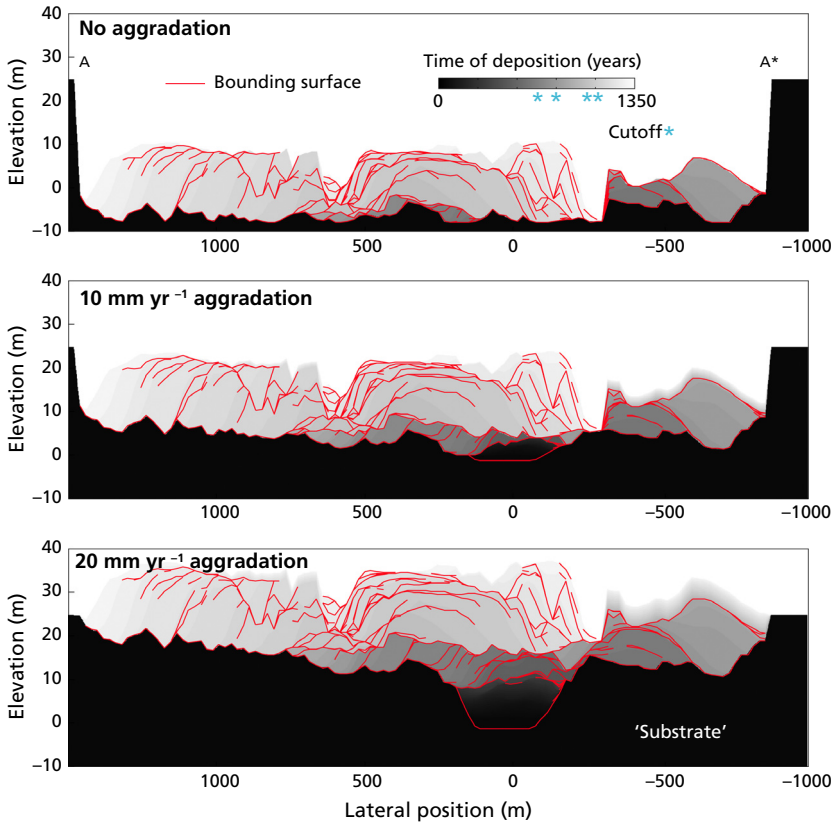

Fig. 5. Synthetic stratigraphy produced by the meander model with and without net aggradation. Slices through this synthetic stratigraphy are analogous to outcrops and can be used to infer time of deposition, channel scour surfaces, set thickness statistics and preservation. The position of the slices is indicated in Figs 4 and 7. Note that the vertical scale has been exaggerated 20 times.

deepest channel structures hosted the thickest sets, of which the tops were reworked by shallower channels again and again. Simulated point bar deposits that were preserved early in the run were often reworked later in the run, primarily in the centre of the meander belt. Ultimately, the succession of the migrating and incising channels and bars determined which part of the scouring history was recorded in the subsurface, with a more complex architecture with many bounding surfaces for a succession of shallower channels and a more straightforward architecture with a limited number of bounding surfaces in those locations where thin deposits were reworked by deeper channels.

Where aggradation was added in the post-processing of the model output (Fig. 5), this obviously increased set thickness but, more importantly, also increased the number of internal bounding surfaces that was preserved. This increase shows that the trade-off between channel and bar migration (as the primary process creating scour surfaces) and bed aggradation (preserving scours in stacked form) determined the preservation of meander morphology.

Effect of bed aggradation

In the main run, most of the meander belt stratigraphic architecture consisted of relatively thin sets, with 50% of the sets being smaller than 2·02 m (Fig. 6A): equal to only 25% of the mean channel depth (h_{mean}) of 8·45 m. The maximum set thickness for this run was 18·5 m, which corresponded to about twice the mean channel depth. The vertical set thickness preservation ratio was 0·36 (Fig. 6B), which indicates that most of the meander belt consisted of fragmented deposits.

The influence of bed aggradation on the stratigraphic architecture was limited for rates smaller than 10 mm yr^{-1} (Fig. 6). Despite an increase in the number of sets from *ca* 9·5 × 10^4 (≈ 3·2 sets per core) for the main model run without aggradation to *ca* 12 × 10^4 (≈ 4·0 sets per core) for a bed aggradation rate of 10 mm yr^{-1}, the median set thickness (Fig. 6A) and vertical set thickness preservation ratio (Fig. 6B) only slightly increased. The variation in set thickness S, quantified by the difference between S_5 and S_{95}, also only increased slightly, which indicates that for bed aggradation rates lower than 10 mm yr^{-1}, most of the added bed elevation was reworked at the same intensity as the zero-aggradation system. Importantly, the architecture that formed as a result of these bed aggradation rates did not differ significantly from the architecture of the main run without net aggradation. This suggests that meander belts formed under net aggradational rates up to 10 mm yr^{-1} cannot be differentiated from equilibrium situations with zero-aggradation based on stratigraphic set thickness distributions logged in field situations.

The influence of bed aggradation on the stratigraphic architecture was more profound for rates exceeding 10 mm yr^{-1} (Fig. 6). Reworking of older deposits decreased and more scour-produced internal bounding surfaces were preserved (Fig. 5). This is well-illustrated by the

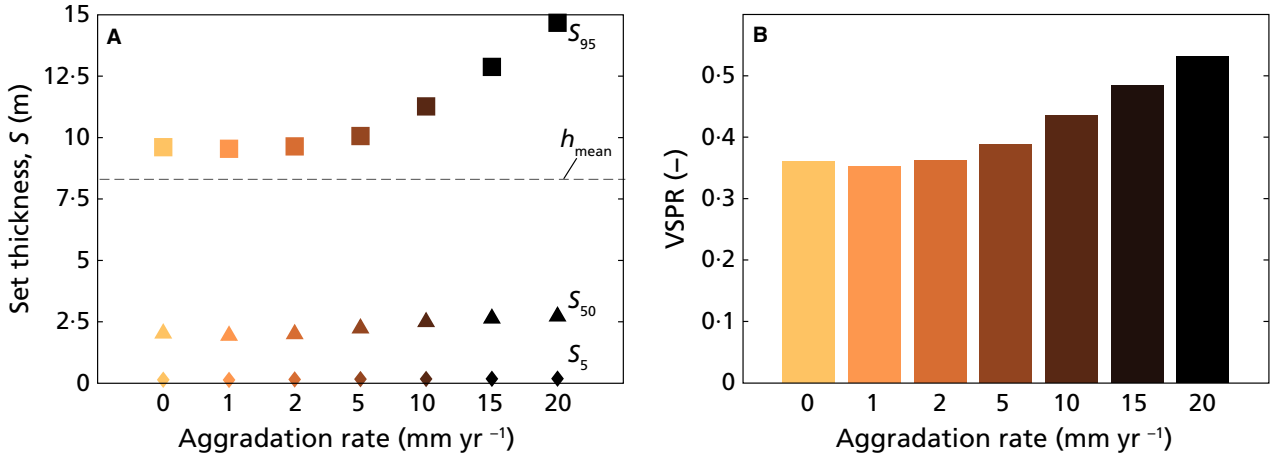

Fig. 6. The effect of aggradation on the stratigraphic architecture of a meander belt. For every virtual core in the model domain stratigraphic set thicknesses (S) were calculated from which a vertical set thickness preservation ratio (*VSPR*) was derived for every run. (A) Stratigraphic set thickness distributions and (B) *VSPR* for different aggradation rates.

number of observed stratigraphic sets, which increased by 27% for a bed aggradation rate of 10 mm yr^{-1} and by 47% for a bed aggradation rate of 20 mm yr^{-1} compared to the main model run without aggradation. The meander belt architecture thus reflects a trade-off between the intensity of channel scouring and bed aggradation. The present authors observed $9{\cdot}5 \times 10^4$ ($\approx 3{\cdot}2$ sets per core) stratigraphic sets for the main model run without bed aggradation. For this zero-aggradation run, the number of stratigraphic sets was merely the result of scour-related variability in topography. For a bed aggradation rate of 10 mm yr^{-1}, *ca* 12×10^4 sets were found ($\approx 4{\cdot}0$ sets per core). In this run, both channel scouring and bed aggradation determined the resultant stratigraphic architecture. For an even higher aggradation rate of 20 mm yr^{-1}, the number of stratigraphic sets further increased to 14×10^4 ($\approx 4{\cdot}7$ sets per core). However, this increase in the number of sets going from 10 to 20 mm yr^{-1} was smaller than the increase in the number of sets going from 0 to 10 mm yr^{-1}, indicating that bed aggradation (preserving scours in stacked form) became the dominant process for rates exceeding 10 mm yr^{-1}.

The bed aggradation rates exceeding 10 mm yr^{-1} also raised the *VSPR* (Fig. 6B): 44% and 53% of the original channel deposit was preserved for bed aggradation rates of 10 mm yr^{-1} and 20 mm yr^{-1}, respectively. These bed aggradation rates thus notably increased the ratio of the channel deposit that was preserved, in contrast to bed aggradation rates lower than 10 mm yr^{-1}, thus demonstrating that reconstructions of the original channel dimensions in principle can more readily be made from stratigraphy for bed aggradation rates of 10 mm yr^{-1} and higher.

It could be argued, however, that the initial time steps in the present modelling corresponded to model spin-up and would exaggerate the difference between the applied bed aggradation rates. Therefore, the set statistics excluding scour surfaces originating from activity before the first simulated cut-off (350 time steps) were also determined. This produced a similar increase in *VSPR* with a slightly higher value (*VSPR* of 56% instead of 53% for an aggradation rate of 20 mm yr^{-1}).

It is worth noting that the stratigraphic differences between the main run with zero-aggradation and the runs with net aggradation were *on average* not that large. For example, the median set thickness only increased from 2·02 m for the run with zero-aggradation to 2·72 m for the run with an extreme bed aggradation rate of 20 mm yr^{-1}. More realistic bed aggradation rates of 1 to 5 mm yr^{-1} resulted in median set thicknesses between 1·94 m and 2·17 m (Fig. 6A), which are very close to the zero-aggradation run. This indicates that for the entire aggradation spectrum, including the extremely high-aggradation rates, most of the stratigraphic architecture consisted of relatively thin sets. However, for the bed aggradation rate of 20 mm yr^{-1} the maximum set thickness was 38·1 m, which is equal to more than twice the maximum set thickness of the run with zero-aggradation, which shows that the spatial *variation* in stratigraphic architecture increased substantially for higher bed aggradation rates (Fig. 6).

Lateral architectural differences

Large spatial differences were observed in meander belt stratigraphic architecture and derived set statistics, with and without bed aggradation (Figs 7 and 8). The systematic behaviour of the meandering channel (i.e. recurring point bar growth, neck cut-off and point bar re-growth) left lateral architectural differences within the meander belt. Relatively undisturbed and largely preserved sets were observed close to meander belt margins and a relatively irregular reworking-influenced stratigraphy of multiple stacked sets in the centre of the meander belt (Figs 7A and 8A). Consequently, sets were on average thicker for the margins than for the centre of the meander belt (Figs 7B and 8B).

Locally, considerable variation in set stacking has also been preserved. For example, single undisturbed sets with a thickness up to 17 m ($\approx 2{\cdot}h_{mean}$) were found in the centre of the meander belt, in the immediate vicinity of stacks of much thinner sets (Fig. 7C). Such occasional thick sets corresponded to abandoned deep meander bends, which had quickly been filled following channel re-routing and had not been reworked since.

Aggradation had a large impact on the lateral architectural differences within the meander belt (Fig. 8A and B). In the axial zone of the meander belt, the number of stacked sets increased from about three for zero aggradation to about six stacked sets for an aggradation signal of 20 mm yr^{-1} (Fig. 8A). At the margins of the meander belt, the number of stacked sets was

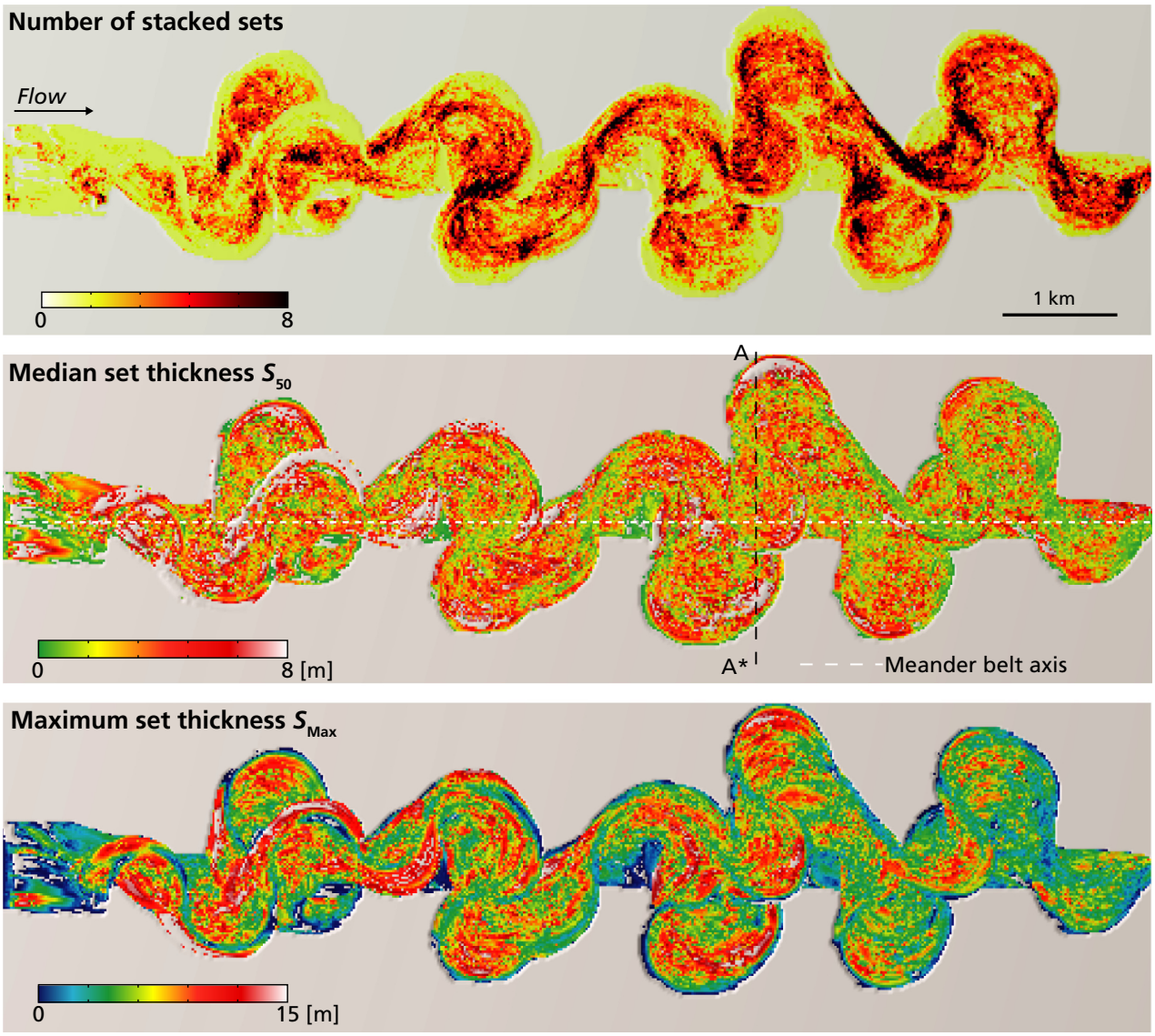

Fig. 7. Map view of the stratigraphic architecture of the simulated meander belt. Set thickness statistics (number of stacked sets, S_{50} and S_{max}) were used to characterize the stratigraphic architecture.

lower with, on average, two stacked sets in a core and was also unaffected by the aggradation signal (Fig. 8A). The median set thickness showed a similar increase from *ca* 4 m for zero aggradation to *ca* 6 m for a 20 mm yr^{-1} aggradation signal from the axial towards the marginal zone (Fig. 8B).

Artificially extended model output (Fig. 4D) showed that the methodology to apply bed aggradation had a significant impact on the lateral expression of architectural differences (Fig. 8C and D). In the axial zone, this extended model output resulted in an increase from about eight stacked sets for zero aggradation to about 28 stacked sets for an aggradation signal of 20 mm yr^{-1} (Fig. 8C). In this extended model output, both scenarios showed a higher number of stacked sets in the axial zone compared to the original main run, reflecting a more mature (i.e. longer activity) meander belt (Fig. 8C). Towards the margins of the meander belt, the number of stacked sets in a core decreased for all aggradation rates to about two stacked sets, similar to the original main run (Fig. 8C).

Interestingly, the extended model output showed an increase in the median set thickness towards the margins for higher bed aggradation rates rather than a homogeneous increase for the entire meander belt as seen in the original main run (Fig. 8D). In the extended model output, the

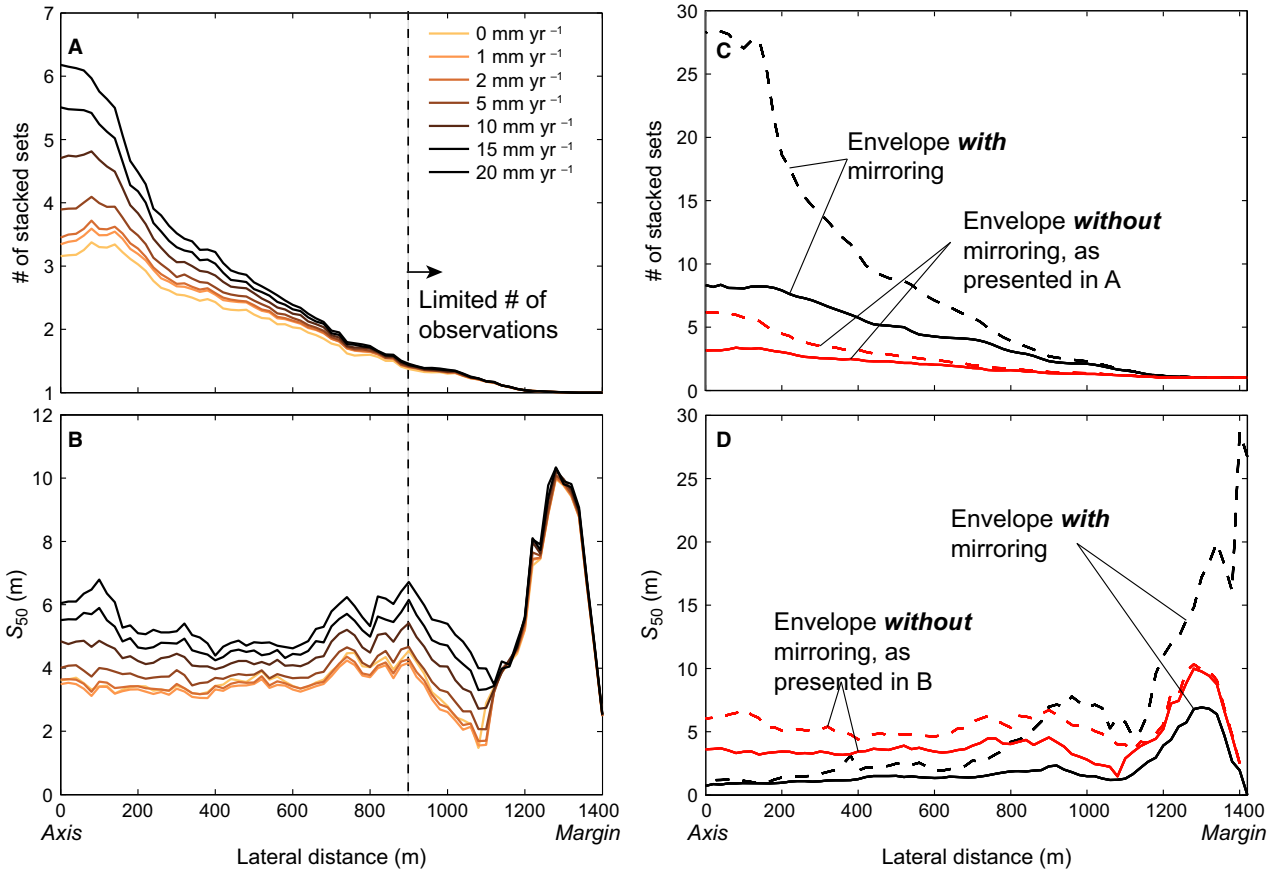

Fig. 8. Lateral differences in stratigraphic architecture within a meander belt for aggrading and non-aggrading conditions. (A) The number of stacked stratigraphic sets as a function of the distance to the meander belt axis for the simulated bed aggradation rates. (B) Median stratigraphic set thickness as a function of the distance to the meander belt axis for the simulated bed aggradation rates. (C) Envelope of the number of stacked sets with and without mirroring, as described in Fig. 4. (D) Envelope of the median stratigraphic set thickness with and without mirroring.

high reworking intensity in the axial zone (Fig. 8C) effectively masked the aggradation signal in the derived set statistics (Fig. 8D). In contrast, deposits were less intensely reworked at the margins (Fig. 8C), thus leaving a clear stratigraphic imprint of aggradation: thicker stratigraphic sets for higher bed aggradation rates (Fig. 8D).

The original as well as the extended model outputs showed that the difference in the number of stacked sets in a core as a function of the aggradation signal decreased towards the margins of a meander belt (Fig. 8C). However, how this was expressed laterally in the meander belt architecture differed (Fig. 8D): in the original model output a laterally homogenous increase in set thickness for higher aggradation rates was observed, while in the extended model output an increase in set thickness towards the margins for higher aggradation rates was seen. Importantly, in the latter case aggradation effectively amplified existing lateral architectural trends as found in non-aggrading meander belts, while in the former case those lateral trends were echoed.

Sensitivity of synthetic architecture

The generated synthetic architectures were the result of the monitoring frequency relative to the rate of process change. Meander belt wide sweeps of the channel are relatively slow and easy to capture while smaller scale bar fluctuations operate at much higher frequencies and require additional composite DEMs for adequate representation in the synthetic architectures and derived set thickness statistics.

A sensitivity analysis demonstrated that the presented preservation of meander morphology, quantified by the *VSPR*, remained similar for a

wide range of the number of composite DEMs included in generating the synthetic stratigraphy (Fig. 9). This indicates that both the slower channel sweeps and faster bar fluctuations were captured adequately.

The sensitivity analysis also revealed a lower limit to the monitoring frequency for which set thickness statistics changed (Fig. 9). If only one-third or less (≤223 DEMs) of the original 668 DEMs were included to generate the synthetic stratigraphy an increase in the *VSPR* was observed. At this lower monitoring frequency, the high-frequency bar fluctuations were no longer captured in the synthetic stratigraphy and fewer bounding surfaces were formed. This logically resulted in an increase in deposit thickness as evidenced by the higher *VSPR*.

DISCUSSION

Comparison with other controlled experiments

The outcomes of current numerical simulations concerning the preservation of meander morphology in aggrading settings are consistent with findings in other controlled experiments. The lack of a clear stratigraphic impact on deposit thickness was also observed in studies on subaqueous bedforms (Leclair *et al.*, 1997; Storms *et al.*, 1999; Leclair, 2002). In agreement with the present results, these earlier studies show that the primary control on deposit thickness is the variability in morphology (for example, channel depth and dune height) and not bed aggradation. For the majority of meandering rivers, the rate of lateral migration (*ca* m yr^{-1}) is orders of magnitude larger than the rate of bed aggradation (*ca* mm yr^{-1}), so it is to be expected that such bed aggradation does not have a significant impact on the preservation of meander morphology.

For extremely high aggradation rates of 10 mm yr^{-1} and higher, the simulations showed increased preservation in agreement with earlier model results replicating migrating subaqueous bedforms (Jerolmack & Mohrig, 2005). In specific settings (for example, confined and vegetated meandering rivers or proximity of an active upstream feeder system) and during short periods of time ($<10^2$ years), it is not unimaginable that aggradation rates may reach 10 mm yr^{-1} and higher. For those specific cases, the current model simulations show that the impact on the affected deposits would be substantial with a significant increase in deposit thickness and preservation. However, field data (e.g. Erkens *et al.*, 2011; Stouthamer *et al.*, 2011) show that such extreme aggradation rates are unlikely to be sustained at a regional scale over 10^3 years and extend beyond the limits found for the majority of natural meandering river systems.

For highly aggradational settings it is also likely that the large amounts of sediment will interact with the meander morphodynamics. Processes currently unaccounted for, such as channel avulsions, may be initiated and overrule the processes incorporated in the current

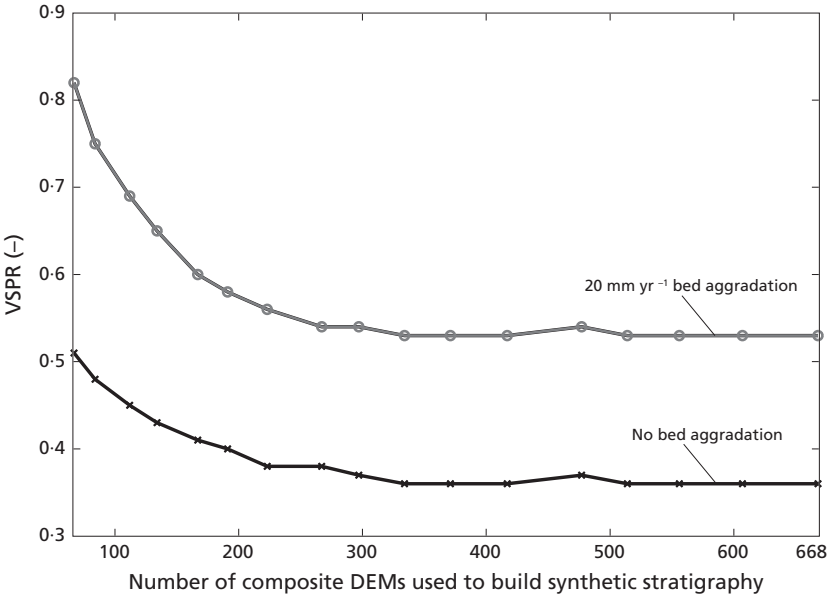

Fig. 9. Insensitivity of the preservation of meander morphology to time resolution. Preservation of meander morphology was quantified by the vertical set thickness preservation ratio (*VSPR*). Note that the set thickness statistics characterizing the stratigraphic architecture are insensitive to the number of composite digital elevation models (DEMs) included to create the synthetic stratigraphy, up to the point that only a third (≈ 223) of the original and total number of 668 composite DEMs was included.

simulation, and thus also result in a different architecture. Flume experiments replicating aggrading braid plains (e.g. Ashworth *et al.*, 2007) have shown a strong positive relationship between aggradation rate and avulsion dynamics. It would be desirable to further examine this relationship for meandering river systems as well in order to obtain more process understanding and to link the current third-order to sixth-order architectural contacts to higher order contacts (Fig. 1).

Comparison with modern and ancient natural meandering river systems

The geometries of the simulated meander belts with aggradation rates up to 10 mm yr^{-1} compare well with reported geometries of ancient and modern meandering systems. A typical meander belt thickness of 6 m for zero aggradation, increasing to *ca* 18 m in the run with an aggradation rate of 10 mm yr^{-1}, combined with an average width of the simulated meander belt of 1250 m, leads to width to thickness ratios ranging from *ca* 70 to 200 in the numerical model. Those ratios are consistent with those reported for a range of ancient meandering systems in Gibling (2006). The ratios also compare well with those reported for a variety of Holocene meander belts within the Rhine–Meuse delta (Gouw & Berendsen, 2007). Although sedimentation conditions are unknown for the meander belts reported in Gibling (2006), it is likely that some of them were formed in aggrading settings.

Conceivably, higher channel belt aggradation could increase the avulsion potential if the floodplain aggradation is not maintained. The present study estimates whether the floodplain aggradation can have followed the meander belt aggradation by a broad-brush analysis of likely bed sediment and floodplain sediment volumes with associated net to gross ratios to compare to typical values in the field. Because volume estimates are quite robust these values are not expected to differ dramatically from more complex situations or from detailed modelling. The volume of the meander belt is simply the thickness multiplied by the width plus aggradation. For the levées, an exponential levée thickness relation is assumed (Fig. 10A; Törnqvist & Bridge, 2002):

$$H_y = H_0 \cdot e^{\frac{-b \cdot y}{y_m}} \quad (1)$$

where H_0 is levée height at the meander belt boundary (m), b is rate of decrease (default is 4), y is distance from meander belt (m) and y_m is characteristic decay length (default 5 km for the Rhine–Meuse delta). Integrating this function

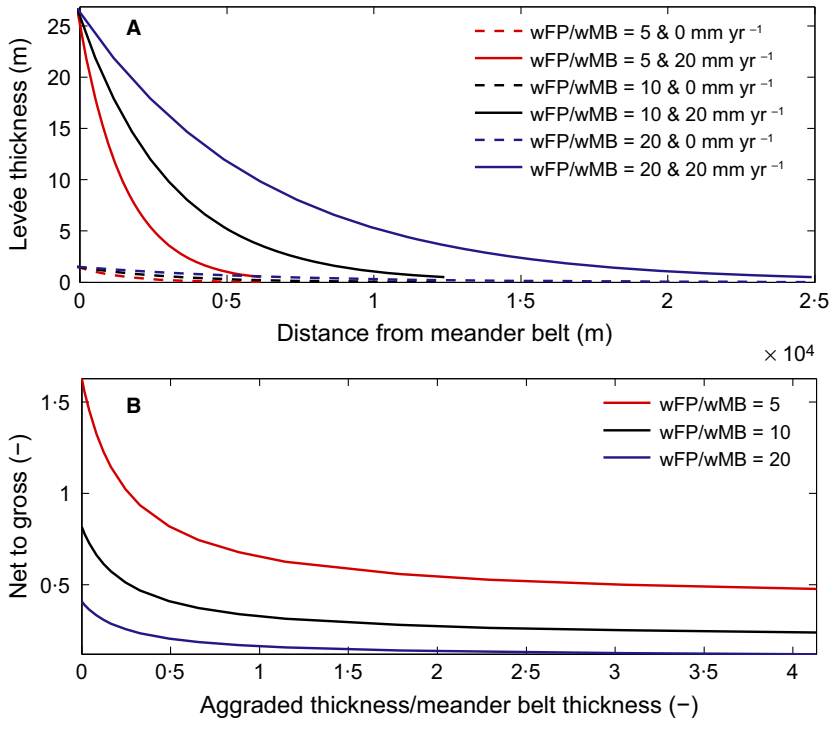

Fig. 10. Estimating net to gross ratios, or sand percentage, for the simulated meander belts. (A) Levée thickness envelopes (see Eq. 1) as a function of the distance from the meander belt for three decay length y_m scenarios (y_m of 6·25 km is equal to 5 wMB, y_m of 12·5 km is equal to 10 wMB, y_m of 25 km is equal to 20 wMB). (B) Net to gross ratios as a function of ratio between aggraded thickness and meander belt thickness.

between distances 0 and y from the meander belt boundary, and multiplying by two for the pair of levées, this results in a relation for levée volume per unit length of channel (Hobo, 2015):

$$L_v = 2 \cdot H_0 \cdot \frac{y_m}{b} \cdot (1 - e^{-b}) \quad (2)$$

Combination with the meander belt volume results in an analytical solution for net to gross as a function of dimensionless ratios of meander belt and levée width and thickness and aggradation thickness relative to meander belt thickness as follows:

$$NG = MB_v / L_v \quad (3)$$

where NG = net to gross, MB_v = ($MB_{thickness}$ + Aggradation) × MB_{width} and L_v = $Levée_{volume}$ (see Eq. 2).

The net to gross ratio is first and foremost a function of the assumed characteristic levée width, which can easily be measured in the field (Fig. 10B). Furthermore, it decreases rapidly with increasing aggradation, because then more floodplain sediment is needed to fill up the higher levées of the aggraded meander belt. Typical net to gross values for floodplain and aggradation characteristics found in natural lowland rivers such as the river Rhine and the lower Mississippi River are of the order 0·4 to 0·8 (e.g. Erkens *et al.*, 2006; Pranter *et al.*, 2007; Hobo, 2015). Therefore, the assumption underlying the model that the river continues to meander because the flanking cohesive floodplains keep up with the aggradation is reasonable.

An angle of climb is present in the synthetic meander belt where the bars build gradually across the belt (Fig. 5). This angle equals the ratio of aggradation over lateral migration. For an aggradation rate of 10 mm yr^{-1}, the angle of climb in the synthetic meander belt was *ca* 0·5° from the horizontal and it doubled to *ca* 1° for an aggradation rate of 20 mm yr^{-1}. This low-angle lateral inclination of meander belts may be useful to obtain an estimate of the aggradational conditions at the time of deposition, although incomplete lateral exposure and autogenic height variations at the base of a meander belt may obscure the low-angle lateral inclination in the field, thus providing an explanation of why this angle is not commonly reported on.

Point bars are the most abundant architectural elements in the preserved synthetic meander belts. This condition is consistent with observations of ancient and modern meandering systems (e.g. Miall, 1985; Ielpi & Ghinassi, 2014) and highlights the relevance of point bars to improve predictive models of meander belts. Ielpi & Ghinassi (2014) report on the expansional and downstream migrating point bar deposits in an exhumed Jurassic meander plain and explicitly relate the occurrence of these point bar styles to the degree of valley confinement, with expansional point bars the dominant mode in meander belts with virtually no confinement and downstream migrating point bars the dominant mode in spatially confined meander belts. In accordance with the association in Ielpi & Ghinassi (2014), the unconfined simulated point bars predominantly showed an expansional style planform migration although most point bars also showed translational and downstream migrating behaviour at some stage in their development.

In addition to affecting the depositional style of point bars, the degree of spatial confinement of meander belts may also affect how aggradation is recorded. With virtually unlimited lateral accommodation, an unconfined expansional meander belt is likely to deposit the majority of the available sediment laterally. This suggests that the internal architectures of expansional meander belts are mostly unaffected by aggradation but instead would be characterized by a high width to thickness ratio of the meander belt. In contrast, spatially confined meander belts are often characterized by a high degree of reworking and low preservation of predominantly downstream migrating point bars (e.g. Alexander *et al.*, 1994; Ielpi & Ghinassi, 2014), thus suggesting that, although the simulated point bars were mostly of the expansional type, the derived set thickness statistics may actually be more representative for spatially confined meander belts with a high degree of reworking and tendency for vertical stacking rather than lateral expansion, particularly for the aggrading runs. The latter assumes that reworking and preservation proceeds in a similar manner for expansional and downstream migrating point bars, which will require further examination.

Observations from meandering systems crossing high-aggradation plains show that individual meander belts mainly consist of lateral accretion deposits. For example, the depositional architecture of aggrading Cenozoic Texas coastal plain fluvial sequences are dominated by belts up to 16 km wide (Galloway, 1981). Similarly, observations from the Miocene Huesca fluvial fan,

Ebro Basin, Spain, show individual meander belt sandstone bodies up to 1·5 km with only a limited thickness up to 5 m (Donselaar & Overeem, 2008). These observations suggest that individual meander belt sandstone bodies on high-aggradation plains are formed primarily by lateral accretion with the majority of the available sediment stored laterally rather than vertically. In turn, this would imply that aggradation has a limited impact on the alluvial architecture of those individual meander belt sandstone bodies, as depicted and statistically described by the main model run with zero-aggradation. However, Galloway (1981) also lists a number of factors including a mixed-load meandering system, long-term stability of the main entry point for sediment input and lateral confinement favouring vertical stacking of point bar deposits, as represented and statistically described by the current runs with post-added aggradation.

Spatial patterns in set thickness variation

The autogenic meandering processes of point bar growth followed by neck cut-off result in large lateral differences in alluvial architecture within meander belts. The current simulations generated synthetic architectures with thick deposits at the margins and thinner deposits in the axial zone of meander belts. Fully preserved channel fills are thus probably found close to the margins of a meander belt, which is consistent with observations in natural (e.g. Lewin & Macklin, 2003) and experimental (van de Lageweg *et al.*, 2013a,b) meandering systems.

Bed aggradation amplifies these autogenic lateral differences in architecture between the margins and axial zone of a meander belt because the aggradation signal is preferentially recorded at the margins. However, the current simulations also show that the strength of this aggradational amplification is highly dependent on how bed aggradation is applied. That is, aggradation was applied uniformly and in conjunction with an expanding meander belt. Clearly, more sophisticated models that include feedbacks between meander dynamics and bed aggradation (e.g. Constantine *et al.*, 2014) are needed in order to make conclusive statements about the impact of aggradation on lateral architectural trends within meander belts.

An emphasis on bounding surfaces, as opposed to sets, provides another link for comparison with the rock record and an avenue to explore lateral architectural differences. Bounding surfaces are erosional breaks in bar and channel-fill aggradation and they generate ground-penetrating radar reflections that can often be used to visualize and evaluate architectural elements (e.g. Miall, 1985; Holbrook, 2001). Figure 5 shows the majority of the bounding surfaces in the axial zone of the simulated meander belts resulting from autocyclic reworking, and also reflective of a higher degree of fragmentation and thinner deposits relative to the margins. Fewer bounding surfaces are observed towards the margins and, more importantly, many bounding surfaces seem to terminate laterally. Thus, there is a transition from a time-hiatus to no-hiatus, and from erosional to aggradational.

This lateral change is caused by morphological as well as temporal change in the meandering river and is likely to be associated with a recognizable signature of sedimentary structures. For example, Reesink & Bridge (2011) relate the abundance and vertical placement of bounding surfaces in unit bars to formative flow conditions and associated sedimentary structures. Similarly, Longhitano & Nemec (2005) find spatial patterns of bed-thickness variation in a Tortorian succession of biocalcarenitic tidal dunes; these statistical tests of bounding surfaces reveal packages of thicker and thinner beds in the axial zone of the depositional system and thinning upward packages at the margins. These authors attribute those lateral differences to the bathymetry of the basin and astronomically driven ebb and flood cycles, although were unable to identify a textural difference between the axial thicker and thinner packages and the thinning upward packages at the margins. Numerical simulations could play a vital role in establishing field-scale relationships between architectural elements, bounding surfaces and sedimentary structure for a range of geomorphic environments by including a range of flow conditions and sediment sizes in future studies.

Implications for the fluvial rock record

The presented stratigraphic set thickness statistics provide quantitative error bounds to reconstruct palaeochannel dimensions from stratigraphy. Zero aggradation defines an important lower bound on the preservation of meander morphology in self-reworking conditions, being close to 36% of the original deposit thicknesses in the NAYS2D simulated meandering system. This *VSPR* is consistent with the

reported ratio of 30% between sets and channel fill for zero-aggradation experimental meandering rivers (van de Lageweg *et al.*, 2013a) and corresponds to low-end predicted ratios of 40% for natural braided rivers (Paola & Borgman, 1991). These field observations, flume experiments and numerical model simulations show that a ratio of *ca* 30% between sets and channel fill is a robust lower bound estimate to reconstruct palaeochannel dimensions from preserved sediments in the absence of aggradation.

For geological successions showing bar and channel scours in river sediments the depositional conditions are typically not known. Exploring the effect of net bed aggradation on stratigraphic architecture and preservation of meander morphology is therefore highly relevant to assess the architectural sensitivity to aggradation. The numerical simulations in the present study highlight that a similar stratigraphic architecture is generated for zero-aggradation up to bed aggradation rates of 10 mm yr^{-1}. Given that net aggradation rates at meander belt scales over 10^3 years are typically in that range, this indicates that fluvial reservoir modelling frameworks will generally not need to modify the stratigraphic architecture within individual meander belts to correct for regional net aggradation. Because the set thickness statistics reflect the rate of lateral migration, i.e. reworking capacity, relative to the rate of aggradation, the results may also be extended to rivers with lower rates of lateral migration and lower rates of aggradation (or higher rates of lateral migration and higher rates of aggradation) compared to the simulated river in this study.

The aforementioned set thickness statistics may be helpful to fully exploit the hydrocarbon and aquifer potential of high-accommodation fluvial basins, which often feature meandering river deposits. A correct description of the internal architecture of meander belt sand bodies is crucial for designing realistic fluvial reservoir architecture models. A well-studied example of such a high-accommodation fluvial basin featuring meandering river deposits is the Pennsylvanian Joggins Formation of Atlantic Canada (Rygel & Gibling, 2006). The Joggins channel deposits were deposited in a rapidly (at least 1 mm yr^{-1}) subsiding basin, in which subsidence is effectively similar to the application of uniform aggradation rates in the current simulations. Despite the rapid subsidence, the meander belt sand bodies in the Joggins Formation show a dominance of lateral accretion deposits organized in a single story of limited thickness and a large lateral extent. This suggests an overall limited impact of subsidence, or aggradation, on the internal architecture of these sand bodies for which the set thickness statistics of the zero to low-end aggradation scenarios in the present study provide quantitative information to populate reservoir models.

This study shows that the sensitivity of the scouring and fragmentation processes are restricted to a specific temporal resolution (Fig. 9); this is as much a function of the processes that were included in the numerical model as it is an indication of what truly matters for sedimentary fragmentation in natural systems. For example, lateral migration and scouring of the meandering channel is relatively slow and generally results in thick deposits while smaller scale bar scouring is a much quicker process resulting in thinner deposits. In this study, composite set thickness distributions consisting of the sedimentary fragments of channel and bar deposits were used. Future studies may identify a specific set thickness distribution for each process individually, which is likely to further current quantitative understanding of preservation mechanisms across a wide range of sedimentary processes and geomorphic settings, in addition to providing tailored quantitative descriptions of specific architectural elements that can be recognized in the fluvial stratigraphic record.

The presented quantitative descriptions of the internal architecture of meander belts may thus be a useful guide to characterize fluvial successions but will require verification through a wider range of case studies. An obvious first step will be to include a range of flow conditions and sediment sizes in future studies. More important, but also more challenging, will be the incorporation of feedbacks between the meander morphodynamics and external signals such as aggradation and subsidence. Including such feedbacks, however, will be crucial to comprehensively quantify the relation between the morphodynamics and architecture of meandering rivers, and may also help to link the third-order to sixth-order intra-channel belt bounding surfaces in this study to larger scale inter channel belt bounding surfaces. Notwithstanding the aforementioned refinements, the current study clearly demonstrates that for low up to extremely high regional net aggradation rates the fundamental control on the internal architecture of a meander belt is the variability in scouring

depth of the meandering channel. Consequently, improving the current ability to reproduce the time-varying and space-varying nature of meander morphology is the most straightforward way to further explore and quantify the preservation of meander morphology.

CONCLUSIONS

The morphodynamic model 'NAYS2D' was used to quantify the effect of bed aggradation on the preservation of meander morphology: NAYS2D is the first numerical model to produce river meandering without presuming a fixed relation between bank erosion and bank accretion, allowing for a more realistic replication of meandering rivers. The simulated highly sinuous meandering river produced stacked depositional features with scoured basal contacts that were related to processes of point bar formation, neck cut-off and in-channel bar scouring.

Model results show no systematic increase in deposit thickness with aggradation rate because the primary control on river channel deposit thickness is the variability in morphology, not aggradation rate. The presented three-dimensional synthetic architectures can be compared directly to the rock record using third-order to sixth-order bounding surfaces.

The systematic behaviour of the meandering channel, i.e. point bar growth followed by neck cut-off, creates lateral architectural differences in meander belts, which are amplified by bed aggradation. Consistent with observations of ancient and modern meandering systems, point bars are the dominant architectural element in the synthetic meander belts, highlighting their relevance to improving predictive models of meander belt architecture. The degree of spatial confinement of meander belts is known to affect the depositional style of point bars and therefore is also likely to affect the recording of aggradation in meander belts. However, with reported meander belt width to thickness ratios typically between 100 and 150 it is clear that most of the architectural variation within meander belts is expected laterally and not vertically, even for highly aggradational meandering systems.

The presented stratigraphic set thickness statistics bear important implications for the architecture of meander belt successions and allow a much more detailed assessment of sand volumes, internal fragmentation and spatial heterogeneity. Such quantitative information is of great value to the characterization of reservoir models to fully exploit the hydrocarbon and aquifer potential.

ACKNOWLEDGEMENTS

We are grateful to reviewers Alessandro Ielpi and Arjan Reesink for their constructive comments. WIvdL was supported by Exxon Mobil Upstream Research Company (grant EM01734 to MGK and G. Postma). MGK, FS and WMvD were supported by the Netherlands Organisation for Scientific Research (NWO) (grant ALW-VIDI-864.08.007 to MGK). Willem Toonen provided much useful discussion and suggestions to improve an earlier version of the manuscript. The authors contributed in the following proportions to conception and study design, model development and data collection, analysis and conclusions, and manuscript preparation: WIvdL (80, 0, 60, 90), FS (0, 50, 10, 0%), KMC (10, 0, 10, 10), WMvD (0, 0, 10, 0), YS (0, 50, 0, 0), MGK (10, 0, 10, 0%).

REFERENCES

Alexander, J., **Bridge, J.S.**, **Leeder, M.R.**, **Collier, R.E.L.L.** and **Gawthorpe, R.L.** (1994) Holocene meander-belt evolution in an active extensional basin, southwestern Montana. *J. Sed. Res.*, **64**, 542–559.

Alexander, J., **Bridge, J.S.**, **Cheel, R.J.** and **Leclair, S.F.** (2001) Bedforms and associated sedimentary structures formed under supercritical water flows over aggrading sand beds. *Sedimentology*, **48**, 33–152.

Allen, J.R.L. (1978) Studies in fluviatile sedimentation: an exploratory quantitative model for the architecture of avulsion-controlled alluvial suites. *Sed. Geol.*, **21**, 129–147.

Allen, J.R.L. (1983) Studies in fluviatile sedimentation: bars, bar-complexes and sandstone sheets (low-sinuosity braided streams) in the brownstones (L. devonian), Welsh borders. *Sed. Geol.*, **33**(4), 237–293.

Allen, J.R.L. (1984) *Sedimentary Structures, Their Character and Physical Basis*. Elsevier Scientific Publishing Company, Amsterdam, 593 pp.

Asahi, K., **Shimizu, Y.**, **Nelson, J.** and **Parker, G.** (2013) Numerical simulation of river meandering with self-evolving banks. *J. Geophys. Res. Earth Surf.*, **118**, 2208–2229.

Ashworth, P.J., **Best, J.L.**, **Peakall, J.** and **Lorsong, J.A.**, 1999. The influence of aggradation rate on braided alluvial architecture: field Study and physical scale-modelling of the Ashburton river gravels, Canterbury plains, New Zealand. In: *Fluvial Sedimentology VI* (Eds N.D. Smith and J. Rogers), pp. 333–346. Blackwell Publishing Ltd., Oxford.

Ashworth, P.J., **Best, J.L.** and **Jones, M.A.** (2004) Relationship between sediment supply and avulsion frequency in braided rivers. *Geology*, **32**, 21–24.

Ashworth, P.J., **Best, J.L.** and **Jones, M.A.** (2007) The relationship between channel avulsion, flow occupancy and aggradation in braided rivers: insights from an experimental model. *Sedimentology*, **54**, 497–513.

Aslan, A. and **Autin, W.J.** (1999) Evolution of the Holocene Mississippi River Floodplain, Ferriday, Louisiana: insights on the origin of fine-grained floodplains. *J. Sed. Res.*, **69**, 800–815.

van Asselen, S., **Stouthamer, E.** and **Smith, N.D.** (2010) Factors controlling peat compaction in alluvial floodplains: a case study in the cold-temperate Cumberland marshes, Canada. *J. Sed. Res.*, **80**, 155–166.

Best, J.L. and **Ashworth, P.J.** (1997) Scour in large braided rivers and the recognition of sequence stratigraphic boundaries. *Nature*, **387**, 275–277.

Bluck, B.J. (1971) Sedimentation in the meandering River Endrick. *Scott. J. Geol.*, **7**, 93–138.

Braudrick, C.A., **Dietrich, W.E.**, **Leverich, G.T.** and **Sklar, L.S.** (2009) Experimental evidence for the conditions necessary to sustain meandering in coarse-bedded rivers. *PNAS*, **106**(16), 936–941.

Bridge, J.S. (1993) Description and interpretation of fluvial deposits: a critical perspective. *Sedimentology*, **40**, 801–810.

Bridge, J.S. and **Best, J.L.** (1997) Preservation of planar laminae due to migration of low-relief bed waves over aggrading upper-stage plane beds: comparison of experimental data with theory. *Sedimentology*, **44**, 253–262.

Bridge, J.S. and **Leeder, M.R.** (1979) A simulation model of alluvial stratigraphy. *Sedimentology*, **26**, 617–644.

Bridge, J.S. and **Mackey, S.D.**, 1993. A revised alluvial stratigraphy model. In: *Alluvial Sedimentation* (Eds M. Marzo and C. Puigdefabregas), *Int. Assoc. Sedimentol. Spec. Publ.*, **17**, 319–336.

Bryant, M., **Falk, P.** and **Paola, C.** (1995) Experimental-study of avulsion frequency and rate of deposition. *Geology*, **23**, 365–368.

Clevis, Q., **de Boer, P.L.** and **Wachter, M.** (2003) Numerical modelling of drainage basin evolution and three-dimensional alluvial fan stratigraphy. *Sed. Geol.*, **163**, 85–110.

Constantine, J.A., **Dunne, T.**, **Ahmed, J.**, **Legleiter, C.** and **Lazarus, E.D.** (2014) Sediment supply as a driver of river meandering and floodplain evolution. *Nat. Geosci.*, **7**, 899–903.

Crosato, A. and **Mosselman, E.** (2009) Simple physics-based predictor for the number of river bars and the transition between meandering and braiding. *Water Resour. Res.*, **45**, W03424.

van Dijk, W.M., **van de Lageweg, W.I.** and **Kleinhans, M.G.** (2012) Experimental meandering river with chute cutoffs. *J. Geophys. Res.*, **117**, F03023.

van Dijk, W.M., **van de Lageweg, W.I.** and **Kleinhans, M.G.** (2013) Formation of a cohesive floodplain in a dynamic experimental meandering river. *Earth Surf. Proc. Land.*, **38**, 1550–1565.

Donselaar, M.E. and **Overeem, I.** (2008) Connectivity of fluvial point-bar deposits: an example from the Miocene Huesca fluvial fan, Ebro Basin, Spain. *AAPG Bull.*, **92**(9), 1109–1129.

Dulal, K.P., **Kobayashi, K.**, **Shimizu, Y.** and **Parker, G.** (2010) Numerical computation of free meandering channels with the application of slump blocks on the outer bends. *J. Hydro-Environ. Res.*, **3**, 239–246.

Eke, E., **Parker, G.** and **Shimizu, Y.** (2014) Numerical modeling of erosional and depositional bank processes in migrating river bends with self-formed width: morphodynamics of bar push and bank pull. *J. Geophys. Res. Earth Surf.*, **119**, 1455–1483.

Engelund, F. (1974) Flow and bed topography in channel bends. *J. Hydraulics Div.*, **100**(11), 1631–1648.

Engelund, F. and **Hansen, E.** (1967) *A Monograph on Sediment Transport in Alluvial Streams*. Teknisk Forlag, Kobenhavn.

Erkens, G., **Cohen, K.M.**, **Gouw, M.J.P.**, **Middelkoop, H.** and **Hoek, W.Z.** (2006) Holocene sediment budgets of the Rhine Delta (The Netherlands): a record of changing sediment delivery. In: *Sediment Dynamics and the Hydromorphology of Fluvial Systems* (Eds J.S. Rowan R.W. Duck & A. Werritty), pp. 406–415. IHAS, Dundee.

Erkens, G., **Dambeck, R.**, **Volleberg, K.P.**, **Bouman, M.T.I.J.**, **Bos, J.A.A.**, **Cohen, K.M.**, **Wallinga, J.** and **Hoek, W.Z.** (2009) Fluvial terrace formation in the northern upper Rhine Graben during the last 20000 years as a result of allogenic controls and autogenic evolution. *Geomorphology*, **103**, 476–495.

Erkens, G., **Hoffmann, T.**, **Gerlach, R.** and **Klostermann, J.** (2011) Complex fluvial response to Lateglacial and Holocene allogenic forcing in the lower Rhine Valley (Germany). *Quatern. Sci. Rev.*, **30**, 611–627.

Ethridge, F.G. (2011) Interpretation of ancient fluvial channel deposits: review and recommendations. In: *From River to Rock Record*, v. 97 (Eds S.K. Davidson, S. Leleu and C.P. North), *SEPM Spec. Publ.*, **97**, 9–35.

Exner, F.M. (1920) Zur physik der dünen. *Akad. Wiss. Wien Math. Naturwiss. Klasse*, **129**2a, 929–952.

Exner, F.M. (1925) Uber die wechselwirkung zwischen wasser und geschiebe in flussen. *Akad. Wiss. Wien Math. Naturwiss. Klasse*, **134**2a, 165–204.

Fisk, H.N. (1944) *Geological Investigation of the Alluvial Valley of the Lower Mississippi River*. Mississippi River Commission, U.S. Corps of Engineers, Vicksburg, MS, 78 pp.

Frascati, A. and **Lanzoni, S.** (2013) A mathematical model for meandering rivers with varying width. *J. Geophys. Res. Earth Surf.*, **118**, 1641–1657.

Friend, P.F., 1983. Towards the field classification of alluvial architecture or sequence. In: *Modern and Ancient Fluvial Systems* (Eds J.D. Collinson and J. Lewin), *IAS Spec. Publ.*, **6**, 345–354.

Galloway, W.E. (1981) Depositional architecture of Cenozoic Gulf coastal plain fluvial systems. *SEPM Spec. Publ.*, **31**, 127–155.

Gibling, M.R. (2006) Width and thickness of fluvial channel bodies and valley fills in the geological record: a literature compilation and classification. *J. Sed. Res.*, **76**, 731–770.

Gouw, M.J.P. (2008) Alluvial architecture of the Holocene Rhine-Meuse delta (The Netherlands). *Sedimentology*, **55**, 1487–1516.

Gouw, M.J.P. and **Berendsen, H.J.A.** (2007) Variability of channel-belt dimensions and the consequences for alluvial architecture: observations from the Holocene Rhine-Meuse delta (The Netherlands) and Lower Mississippi Valley (USA). *J. Sed. Res.*, **77**(2), 124–138.

Heller, P.L. and **Paola, C.** (1996) Downstream changes in alluvial architecture: an exploration of controls on channel-stacking patterns. *J. Sed. Res.*, **66**, 297–306.

Hobo, N. (2015) The sedimentary dynamics in natural and human-influenced delta channel belts. *Utrecht Stud Earth Sci.*, **97**, 200.

Holbrook, J. (2001) Origin, genetic interrelationships, and stratigraphy over the continuum of fluvial channel-form bounding surfaces: an illustration from middle Cretaceous strata, south eastern Colorado. *Sed. Geol.*, **144**, 179–222.

Hudson, P.F. and **Kesel, R.H.** (2000) Channel migration and meander-bend curvature in the lower Mississippi River prior to major human modification. *Geology*, **28**, 531–534.

Ielpi, A. and **Ghinassi, M.** (2014) Planform architecture, stratigraphic signature and morphodynamics of an exhumed Jurassic meander plain (Scalby Formation, Yorkshire, UK). *Sedimentology*, **61**, 1923–1960.

Jang, C. and **Shimizu, Y.** (2005) Numerical simulation of relatively wide shallow channels with erodible banks. *J. Hydraulic Eng.*, **131**, 565–575.

Jerolmack, D.J. and **Mohrig, D.** (2005) Frozen dynamics of migrating bedforms. *Geology*, **33**(1), 57–60.

Kleinhans, M.G. (2010) Sorting out river channel patterns. *Prog. Phys. Geogr.*, **34**, 287–326.

Kleinhans, M.G. and **van den Berg, J.H.** (2011) River channel and bar patterns explained and predicted by an empirical and a physics-based method. *Earth Surf. Proc. Land.*, **36**, 721–738.

Kleinhans, M.G., **Jagers, H.R.A.**, **Mosselman, E.** and **Sloff, C.J.** (2008) Bifurcation dynamics and avulsion duration in meandering rivers by one-dimensional and three-dimensional models. *Water Resour. Res.*, **44**, W08454.

Kleinhans, M.G., **Cohen, K.M.**, **Hoekstra, J.** and **IJmker, J.M.** (2011) Evolution of a bifurcation in a meandering river with adjustable channel widths, Rhine delta apex, The Netherlands. *Earth Surf. Proc. Land.*, **36**, 2011–2027.

Kleinhans, M.G., **van Dijk, W.M.**, **van de Lageweg, W.I.**, **Hoyal, D.C.J.D.**, **Markies, H.**, **van Maarseveen, M.**, **Roosendaal, C.**, **van Weesep, W.**, **van Breemen, D.**, **Hoendervoogt, R.** and **Cheshier, N.** (2014) Quantifiable effectiveness of experimental scaling of river- and delta morphodynamics and stratigraphy. *Earth-Sci. Rev.*, **133**, 43–61.

van de Lageweg, W.I., **van Dijk, W.M.** and **Kleinhans, M.G.** (2013a) Channel belt architecture formed by a meandering river. *Sedimentology*, **60**, 840–859.

van de Lageweg, W.I., **van Dijk, W.M.** and **Kleinhans, M.G.** (2013b) Morphological and stratigraphical signature of floods in a braided gravel-bed river revealed from flume experiments. *J. Sed. Res.*, **83**, 1032–1045.

van de Lageweg, W.I., **van Dijk, W.M.**, **Baar, A.W.**, **Rutten, J.** and **Kleinhans, M.G.** (2014) Bank pull or bar push: what drives scroll-bar formation in meandering rivers? *Geology*, **42**, 319–322.

Lane, S.N. (1997) The reconstruction of bed material yield and supply histories in gravel-bed streams. *Catena*, **30**, 183–196.

Lane, S.N., **Richards, K.S.** and **Chandler, J.H.** (1994) Developments in monitoring and terrain modelling of small-scale riverbed topography. *Earth Surf. Proc. Land.*, **19**, 349–368.

Lanzoni, S. and **Seminara, G.** (2006) On the nature of meander instability. *Water Resour. Res.*, **111**, F04006.

Leclair, S.F. (2002) Preservation of cross-strata due to the migration of subaqueous dunes: an experimental investigation. *Sedimentology*, **49**, 1157–1180.

Leclair, S.F. and **Bridge, J.S.** (2001) Quantitative interpretation of sedimentary structures formed by river dunes. *J. Sed. Res.*, **71**, 713–716.

Leclair, S.F., **Bridge, J.S.** and **Wang, F.** (1997) Preservation of cross-strata due to migration of subaqueous dunes over aggrading and non-aggrading beds: comparison of experimental data with theory. *Geosci. Can.*, **24**, 55–66.

Leeder, M. (1978) A quantitative stratigraphic model for alluvium, with special reference to channel deposit density and interconnectedness. In: *Fluvial Sedimentology* (ed. A.D. Miall), *Can. Soc. Petrol. Geol. Mem.*, **5**, 587–596.

Lesser, G., **Roelvink, J.**, **van Kester, J.** and **Stelling, G.** (2004) Development and validation of a three-dimensional morphological model. *Coast. Eng.*, **51**, 883–915.

Lewin, J. and **Macklin, M.G.** (2003) Preservation potential for Late Quaternary river alluvium. *J. Quatern. Sci.*, **18**, 107–120.

Longhitano, S.G. and **Nemec, W.** (2005) Statistical analysis of bed-thickness variation in a Tortorian succession of biocalcarenitic tidal dunes, Amantea Basin, Calabria, southern Italy. *Sed. Geol.*, **179**, 195–224.

Mackey, S.D. and **Bridge, J.S.** (1995) Three-dimensional model of alluvial stratigraphy: theory and application. *J. Sed. Res.*, **B65**(1), 7–31.

Miall, A.D. (1985) Architectural-element analysis: a new method of facies analysis applied to fluvial deposits. *Earth Sci. Rev.*, **22**, 261–308.

Middelkoop, H. and **Asselman, N.E.M.** (1998) Spatial variability of floodplain sedimentation at the event scale in the Rhine-Meuse delta, the Netherlands. *Earth Surf. Proc. Land.*, **23**, 561–573.

Murray, A.B. and **Paola, C.** (1994) A cellular model of braided rivers. *Nature*, **371**, 54–57.

North, C.P. (1996) The prediction and modelling of subsurface fluvial stratigraphy. In: *Advances in Fluvial Dynamics and Stratigraphy* (Eds P.A. Carling and M.R. Dawson), pp. 395–508. John Wiley and Sons, Chichester.

Paola, C. and **Borgman, L.** (1991) Reconstructing random topography from preserved stratification. *Sedimentology*, **38**, 553–565.

Paola, C., **Mullin, J.**, **Ellis, C.**, **Mohrig, D.C.**, **Swenson, J.B.**, **Parker, G.**, **Hickson, T.**, **Heller, P.L.**, **Pratson, L.**, **Syvitski, J.**, **Sheets, B.** and **Strong, N.** (2001) Experimental stratigraphy. *GSA Today*, **11**(7), 4–9.

Paola, C., **Straub, K.M.**, **Mohrig, D.C.** and **Reinhardt, L.** (2009) The 'unreasonable effectiveness' of stratigraphic and geomorphic experiments. *Earth Sci. Rev.*, **97**, 1–43.

Paola, C. and **Voller, V.R.** (2005) A generalized Exner equation for sediment mass balance. *J. Geophys. Res. Earth Surf.*, **110**, F04014.

Parker, G., **Shimizu, Y.**, **Wilkerson, G.V.**, **Eke, E.C.**, **Abad, J.D.**, **Lauer, J.W.**, **Paola, C.**, **Dietrich, W.E.** and **Voller, V.R.** (2011) A new framework for modeling the migration of meandering rivers. *Earth Surf. Proc. Land.*, **36**, 70–86.

Pranter, M.J., **Ellison, A.I.**, **Cole, R.D.** and **Patterson, P.** (2007) Analysis and modeling of intermediate-scale reservoir heterogeneity based on a fluvial point-bar outcrop analog, Williams Fork Formation, Piceance Basin, Colorado. *AAPG Bull.*, **91**, 1025–1051.

Reesink, A.J.H. and **Bridge, J.S.** (2011) Evidence of bedform superimposition and flow unsteadiness in unit-bar deposits, South Saskatchewan River, Canada. *J. Sed. Res.*, **81**, 814–840.

van Rijn, L.C. (1984) Sediment transport, part iii: bed forms and alluvial roughness. *J. Hydraulic Eng.*, **110**(12), 1733–1754.

Rygel, M.C. and **Gibling, M.R.** (2006) Natural geomorphic variability recorded in a high-accomodation setting: fluvial

architecture of the Pennsylvanian Joggins Formation of Atlantic Canada. *J. Sed. Res.*, **76**, 1230–1251.

Sadler, P.M. (1981) Sediment accumulation rates and the completeness of stratigraphic sections. *J. Geol.*, **89**, 569–584.

Schumm, S.A. (1985) Patterns of alluvial rivers. *Annu. Rev. Earth Planet. Sci.*, **13**, 5–27.

Schuurman, F. and **Kleinhans, M.G.** (2015) Morphodynamic modeling of bar dynamics and bifurcation evolution in a braided sand-bed river. *Earth Surf. Proc. Land.*, **40**, 1318–1333.

Schuurman, F., **Kleinhans, M.G.** and **Marra, W.A.** (2013) Physics-based modeling of large braided sand-bed rivers: bar pattern formation, dynamics, and sensitivity. *J. Geophys. Res. Earth Surf.*, **118**, 2509–2527.

Schuurman, F., **Shimizu, Y.**, **Iwasaki, T.** and **Kleinhans, M.G**. (2015) Dynamic perturbation in response to upstream perturbation and floodplain formation. *Geomorphology*, doi:10.1016/j.geomorph.2015.05.039.

Smith, N.D. (1971) Transverse bars and braiding in the lower Platte River, Nebraska. *Bull. Geol. Soc. Am.*, **82**, 3407–3420.

Storms, J.E.A., **Dam, R.L.V.** and **Leclair, S.F.** (1999) Preservation of cross-sets due to migration of current ripples over aggrading and non-aggrading beds: comparison of experimental data with theory. *Sedimentology*, **46**, 189–200.

Stouthamer, E. and **Berendsen, H.J.A.** (2000) Factors controlling the holocene avulsion history of the Rhine-Meuse Delta, The Netherlands. *J. Sed. Res.*, **70**(5), 1051–1064.

Stouthamer, E., **Cohen, K.M.** and **Gouw, M.J.P**. (2011) From River to Rock Record: The preservation of fluvial sediments and their subsequent interpretation. In: *Avulsion and its Implications for Fluvial-Deltaic Architecture, insight from the Rhine-Meuse Delta* (Eds S.K. Davidson S. Leleu and C.P. North), *SEPM Spec. Publ.*, **97**, 215–231.

Terry, J.P., **Garimella, S.** and **Kostaschuk, R.A.** (2002) Rates of floodplain accretion in a tropical island river system impacted by cyclones and large floods. *Geomorphology*, **42**, 171–182.

Törnqvist, T.E. and **Bridge, J.S.** (2002) Spatial variation of overbank aggradation rate and its influence on avulsion frequency. *Sedimentology*, **49**, 891–905.

Tyler, N. and **Finley, R.J**. (1991) Architectural controls on the recovery of hydrocarbons from sandstone reservoir. In: *The Three-Dimensional Facies Architecture of Terrigenous Clastic Sediments and its Implications for Hydrocarbon Discovery and Recovery* (Eds A.D. Miall and N. Tyler), *SEPM Concepts Sedimentol. Paleontol.*, **3**, 1–5.

Walling, D.E. and **He, Q.** (1997) Investigating spatial patterns of overbank sedimentation on river floodplains. *Water Air Soil Pollut.*, **99**, 9–20.

Willis, B.J. and **Tang, H.** (2010) Three-dimensional connectivity of point-bar deposits. *J. Sed. Res.*, **80**, 440–454.

Zolezzi, G., **Luchi, R.** and **Tubino, M**. (2012) Modeling morphodynamic processes in meandering rivers with spatial width variations. *Rev. Geophys.*, **50**, RG4005.

Manuscript received 30 January 2015; revision accepted 20 August 2015